nature plants

Article

https://doi.org/10.1038/s41477-025-01942-w

Hordeum I genome unlocks adaptive evolution and genetic potential for crop improvement

Received: 24 October 2023

Accepted: 11 February 2025

Published online: 14 March 2025

Check for updates

Hao Feng[1,6], Qingwei Du[1,6], Ying Jiang[1,6], Yong Jia[2,6], Tianhua He[2], Yibin Wang[3], Brett Chapman[2], Jiaxin Yu[3], Haiwen Zhang[1], Mengxue Gu[1], Mengwei Jiang[3], Shanshan Gao[1], Xinjie Zhang[1], Yameng Song[1], Vanika Garg[4], Rajeev K. Varshney[4], Jianhua Wei[1] ✉, Chengdao Li[2,4,5] ✉, Xingtan Zhang[3] ✉ & Ruifen Li[1] ✉

Crop wild relatives (CWRs) are invaluable for crop improvement. Among these, *Hordeum* I-genome species exhibit exceptional tolerance to alkali and salt stresses. Here we present a chromosome-scale genome assembly of *Hordeum brevisubulatum* (II, $2n = 2x = 14$) and genome resequencing of 38 diploid germplasms spanning 7 I-genome species. We reveal that the adaptive evolution of the *H. brevisubulatum* genome is shaped by structural variations, some of which may contribute to its adaptation to high alkali and salt environments. Evolutionary duplication of the stress sensor-responder module CaBP-NRT2 and the horizontally transferred fungal gene *Fhb7* were identified as novel alkaline–saline tolerance mechanisms. We also demonstrate the potential of the *Hordeum* I genome in crop breeding through the newly synthesized hexaploid *Tritordeum* (AABBII) with enhanced alkaline–saline tolerance. Our study fills critical gaps in *Hordeum* genomics and CWR research, advancing introgression of CWR resources into current crops for sustainable agriculture.

Agronomy innovations and crop breeding have been instrumental in achieving sustained growth in global food production over the past century. However, ensuring food security for a growing population remains a major challenge, especially due to climate change and limited genetic resources[1–3]. Breeding efforts to develop genetically uniform cultivars have focused on a narrow pool of species and varieties, overlooking a wealth of locally adapted and genetically diverse traditional crops. While modern breeding, through prolonged domestication, has enhanced traits that boost productivity, it has also led to genetic bottlenecks, reducing genetic diversity and stress resistance in modern crop gene pools[4]. Crop wild relatives (CWRs) are reservoirs of valuable traits, including diverse forms of resistance to biotic and abiotic stresses, which are critical for adapting modern cultivars to future climate conditions[5,6]. Harnessing the genetic diversity of CWRs to improve stress resistance is paramount for future crop breeding efforts[7].

[1]Beijing Key Laboratory of Agricultural Genetic Resources and Biotechnology, Institute of Biotechnology, Beijing Academy of Agriculture and Forestry Sciences, Beijing, China. [2]Western Crop Genetic Alliance/the State Agricultural Biotechnology Centre, College of Science, Health, Engineering and Education, Murdoch University, Murdoch, Western Australia, Australia. [3]National Key Laboratory for Tropical Crop Breeding, Shenzhen Branch, Guangdong Laboratory for Lingnan Modern Agriculture, Genome Analysis Laboratory of the Ministry of Agriculture, Agricultural Genomics Institute at Shenzhen, Chinese Academy of Agricultural Sciences, Shenzhen, China. [4]Centre for Crop & Food Innovation, WA State Agricultural Biotechnology Centre, Food Futures Institute, Murdoch University, Murdoch, Western Australia, Australia. [5]Department of Primary Industries and Regional Development, South Perth, Western Australia, Australia. [6]These authors contributed equally: Hao Feng, Qingwei Du, Ying Jiang, Yong Jia. ✉e-mail: weijianhua@baafs.net.cn; c.li@murdoch.edu.au; zhangxingtan@caas.cn; liruifen@babrc.ac.cn

Plants in the Triticeae tribe include some of the world's most important cereal crops, such as wheat and barley, providing a substantial portion of global dietary intake. Among Triticeae CWRs, *Hordeum* I-genome species have garnered attention due to their exceptional stress tolerance and genetic diversity[8–10]. Species such as *Hordeum brevisubulatum* show superior adaptability to saline and alkaline soils[11,12]. With over one billion hectares of arable land worldwide affected by salt toxicity, approximately 60% of which is sodic[13], transferring adaptive traits from *Hordeum* I-genome species into crops holds considerable promise for improving stress resilience in modern barley and wheat varieties. While considerable progress has been made in understanding the mechanisms behind plant salt tolerance, knowledge of alkaline salinity (alkali) tolerance remains limited. Alkali stress is more detrimental to plant growth than neutral salinity stress, particularly by reducing the uptake of essential nutrients and exacerbating oxidative stress[14]. Proteins with the evolutionarily conserved EF-hand motif—such as calmodulin and calmodulin-like—sense stress-triggered Ca^{2+} signals, thereby coordinating stress response pathways[15,16]. However, it is unknown whether novel Ca^{2+}-binding proteins (CaBPs) specifically respond to alkali stress and enhance nutrient uptake for plant survival. In addition, horizontal gene transfer (HGT) events have been shown to contribute to plant adaptation[17,18], yet the role of HGT-derived genes in the adaptation of Triticeae CWRs to saline–alkaline stress remains unclear.

To address these gaps, we de novo assembled a chromosome-scale genome for *H. brevisubulatum* (I genome) using PacBio high-fidelity (HiFi) long-read sequencing and high-throughput chromatin conformation capture (Hi-C). We performed whole-genome resequencing of 38 accessions from seven I-genome species, followed by comparative and population-based structural variations analyses with *Hordeum marinum* and *Hordeum vulgare*. Our findings reveal remarkable genomic rearrangements that have shaped the evolution and environmental adaptation of the I-genome species. We identified and functionally verified key candidate genes contributing to the superior alkali and salinity stress resistance of *H. brevisubulatum*. Furthermore, we evaluated the genetic potential of the I genome for crop improvement via a newly synthesized hexaploid species, *Tritordeum* (AABBII, $2n = 6x = 42$), which features a substituted I-subgenome and shows enhanced alkaline–saline tolerance. Our study lays the foundation for *Hordeum* I-genome research, enhancing the potential for transferring elite I-genome alleles into future wheat and barley breeding programs to address global food security challenges under climate change.

Results

Genome assembly and composition

A superior alkaline–saline tolerant *H. brevisubulatum* line (accession PI 531775, $2n = 2x = 14$) was selected for reference genome sequencing (Extended Data Fig. 1a,b). The genome size and ploidy were determined through flow cytometry analysis (Extended Data Fig. 1c and Supplementary Fig. 1). This I-genome accession exhibits a perennial growth habit, early spring regrowth and increased tiller numbers compared to the previous year's growth (Extended Data Fig. 1d–f). To generate a high-quality reference genome, we used 45× PacBio HiFi sequencing and 158× Hi-C reads (Extended Data Fig. 1g). The assembly yielded 3.47 Gb of genome sequence, with a contig N50 size of 82.35 Mb and a scaffold N50 size of 476.19 Mb (Supplementary Table 1), accounting for 96.66% of the estimated genome size (3.59 Gb by *K*-mer; Extended Data Fig. 1h). Of the total assembly, 3.39 Gb (94.35%) were anchored and oriented into seven pseudo-chromosomes (1I–7I). The long terminal repeat (LTR) assembly index score of 22.98 for this assembly surpasses that of *H. marinum* (12.94) and *H. vulgare* (15.91) (Supplementary Table 2), indicating superior genome contiguity. In total, 73,672 protein-coding genes were annotated, with 99.4% mapped to the seven pseudo-chromosomes. Benchmarking Universal Single-Copy Orthologs (BUSCO) analysis identified 94.64% of complete Poales genes in the *H. brevisubulatum* assembly, further confirming its completeness (Supplementary Tables 1 and 2). Gene distribution analysis revealed a concentration of annotated genes in the distal chromosomal regions, where transposable elements were less abundant (Fig. 1a).

Genomic evolution and features

The evolutionary relationship of the *H. brevisubulatum* I genome with other sequenced genomes within Triticeae (*Secale cereale*, *Thinopyrum elongatum*, *Aegilops tauschii*, *Triticum urartu*, *Aegilops speltoides*, *Triticum aestivum*, *H. vulgare*, *Hordeum spontaneum* and *H. marinum*), Aveneae (*Avena sativa*), and Poeae (*Puccinellia tenuiflora*) was resolved using a maximum likelihood phylogenetic tree based on 268 single-copy genes (Fig. 1b). *H. brevisubulatum* (I genome) was more closely related to *H. marinum* (Xa genome) than to *H. vulgare* (H genome) within the *Hordeum* clade. Divergence time estimation suggests that *H. brevisubulatum* split from *H. marinum* (sea barleygrass) approximately 5.34 Ma during the latest Miocene. Synonymous substitution distribution and fourfold degenerate site transversion (4dTv) confirmed a whole-genome duplication event in the Pooideae ancestor and identified a recent burst of gene duplication specific to Triticeae species[19] (Extended Data Fig. 1i, j).

The *H. brevisubulatum* genome has a lower transposable element content (83.60%, 2.90 Gb) than *H. marinum* (86.74%, 3.31 Gb) and *H. vulgare* (88.44%, 3.71 Gb) (Supplementary Table 3), corresponding to a reduction of approximately 410 Mb and 810 Mb, respectively. As transposable element content substantially influences genome size in Triticeae[20,21], this reduction likely makes *H. brevisubulatum* the smallest among sequenced diploid *Hordeum* species. Despite the lower transposable element content, the LTR retrotransposon (LTR-RT) subfamilies *Fatima*, *Inga*, *Nusif*, and *Angala* expanded substantially in *H. brevisubulatum* compared to *H. marinum* and *H. vulgare* (Extended Data Fig. 1k). Comparative analysis of transposable element insertion sites among the three *Hordeum* reference genomes revealed distinct patterns in *H. brevisubulatum*. LTR-RTs occurred most frequently adjacent to gene bodies (Fig. 1c), while DNA transposons were enriched in the upstream and downstream 5 kb regions but occurred less frequently near gene bodies (Fig. 1d). In addition, *H. brevisubulatum* exhibited higher proportions of tandem duplication, proximal duplication and transposed duplication (Supplementary Table 4), correlating with increased transposable element occurrence (Fig. 1e). Orthologous gene analysis across Triticeae, Aveneae and Poeae identified 3,602 genes unique to *H. brevisubulatum* (Supplementary Table 5 and Extended Data Fig. 1m). These genes were enriched in Gene Ontology (GO) categories related to cellular nitrogen metabolism and cellulose catabolism (Supplementary Data 1), suggesting their role in the adaptive evolution of *H. brevisubulatum*. It is worth noting that the *FAR1* transcription factor gene family, associated with environmental adaptation[22], exhibited exceptional expansion in *H. brevisubulatum* (Extended Data Fig. 1l and Supplementary Data 2), with several genes showing differential expression under salt or alkali stress (Supplementary Data 2).

Structural variation analysis between *H. brevisubulatum*, *H. marinum* and *H. vulgare* genomes revealed that megabase-scale inversions accounted for 78.6% of all inversions (Fig. 1f). Notable gene expansion events associated with large structural variations were observed on chromosomes 1I (8.27–46.16 Mb) and 7I (29.59–65.33 Mb; 504.96–524.83 Mb) of the *H. brevisubulatum* genome compared to *H. marinum* and *H. vulgare*. GO enrichment analysis showed that these expanded genes are related to stress, stimulus and defence responses and disease resistance (Supplementary Data 3). Furthermore, genes within 300 kb of inversion breakpoints in *H. brevisubulatum* were enriched in defence-related functions (Supplementary Data 4), such as those in the NB-ARC (nucleotide-binding adaptor shared by APAF-1, R proteins and CED-4) family (Supplementary Data 5) associated with disease resistance[23]. This enrichment was absent in the corresponding regions in *H. marinum* and *H. vulgare* (Supplementary Data 4).

https://doi.org/10.1038/s41477-025-01942-w

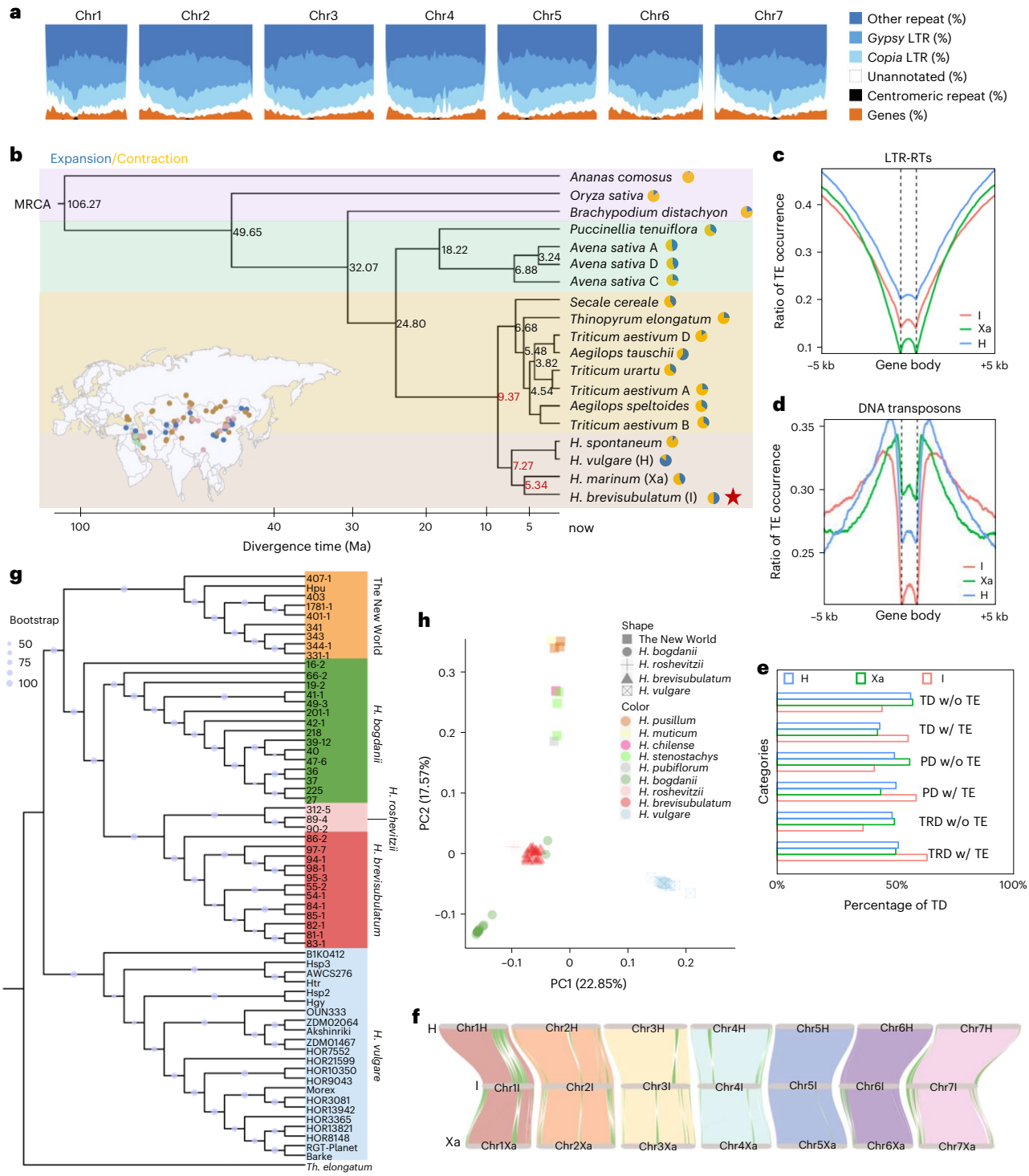

Fig. 1 | Evolution, feature, and genomic diversity of the I genome. a, Genomic features of *H. brevisubulatum*. The proportion of LTR-RTs (including *Gypsy* and *Copia*, two major families of LTR-RTs), other repeats, genes, unannotated regions and centromeric repeats are represented. **b**, Phylogenetic relationship of 19 genomes, including I genome and other available Triticeae genomes. The divergence times among different species are labelled on the branch point. The numbers on each apex represent gene families' expansion (dark blue) and contraction (orange). The star indicates *H. brevisublatum* assembled in this study. Divergence time points among *Hordeum* species are marked in red. The left lower part represents the geographical distribution of *H. brevisubulatum* accessions with different ploidies (Supplementary Data 10). Pink dots, $2n = 14$; blue dots, $2n = 28$; green dots, $2n = 42$; brown dots, ploidies unknown. **c**,**d**, The occurrence of LTR-RTs (**c**) and DNA transposons (**d**) in the upstream and downstream (-5 kb) gene regions in the genomes of *H. brevisubulatum*, *H. marinum* and *H. vulgare*. **e**, Percentage of tandem duplication (TD), proximal duplication (PD) and transposed duplication (TRD) with (w/) and without (w/o) transposable elements (TE) in the genomes of *H. brevisubulatum*, *H. marinum* and *H. vulgare*. **f**, Synteny analysis among *H. brevisubulatum* (representing the I genome), *H. vulgare* (representing the H genome) and *H. marinum* (representing the Xa genome) by chromosomal positions. Inversions are highlighted in green. **g**, The phylogenetic tree of 62 accessions was constructed using SNPs of whole-genome single-copy genes. The 61 *Hordeum* accessions are clustered into five groups: *H. brevisubulatum*, *H. roshevitzii*, *H. bogdanii*, the New Word group and *H. vulgare*. *T. elongatum* was set as the out-group. The sizes of the dots on the nodes are proportional to bootstrap support values. **h**, PCA of 61 accessions (including 12 *H. brevisubulatum*, 15 *H. bogdanii*, 3 *H. roshevitzii*, 9 accessions from the New World and 22 barley accessions). The classifications of species are represented by shapes or colours.

Comparisons with the 20-barley pan-genome revealed additional structural-variation-related gene expansions in *H. brevisubulatum* (Supplementary Fig. 2 and Supplementary Data 6). It is worth noting that a gene (*HorBre03H01G096680*) orthologous to *Cul4* in barley and *tin3* in wheat, both associated with tillering[24–26], was identified near the breakpoint of a 674 kb inversion on chromosome 3IL.

Population structure and genomic diversity

To explore the genetic diversity and evolutionary patterns of the I genome, we resequenced 38 diploid accessions, including 12 *H. brevisubulatum*, 15 *Hordeum bogdanii*, three *Hordeum roshevitzii* and eight from four New World species (*Hordeum chilense*, *Hordeum muticum*, *Hordeum pusillum* and *Hordeum stenostachys*) (Supplementary Data 7). In addition, we incorporated previously published resequencing data for 22 H-genome accessions and one I-genome accession[27–30] (Supplementary Data 7), identifying 2,209,666 high-quality single-nucleotide polymorphisms (SNPs) across all accessions. Phylogenetic analyses (Fig. 1g), principal component analysis (PCA; Fig. 1h and Extended Data Fig. 2b) and population structure assessments (Extended Data Fig. 2a) revealed three major clades among the I-genome species, reflecting species-level differentiation and evolutionary relationships. Clades I and II comprised *H. brevisubulatum*, *H. bogdanii* and *H. roshevitzii* from the Old World, while the more divergent Clade III contained New World species. It is worth noting that three accessions (IDs 27, 201-1 and 19-2) previously classified as *H. brevisubulatum* in the US National Plant Germplasm System (NPGS) were reassigned to *H. bogdanii* based on phylogenetic and field-based phenotypic data (Supplementary Data 7). Similarly, two highly heterozygous accessions (16-2 and 66-2) previously recorded as *H. brevisubulatum* were found to have predominantly *H. bogdanii* genomic background in the population structures analyses (Extended Data Fig. 2a). Discrepancies in clustering for some accessions (for example, 407-1, 1781-1 and 331-1) highlight the need for further investigation, including morphological examination and chloroplast genome sequencing.

The outcrossing *H. brevisubulatum* exhibited the highest nucleotide diversity ($\pi = 3.43 \times 10^{-4}$) among the analysed I- and H-genome species (Supplementary Table 6). Evidence of introgression from *H. brevisubulatum* to *H. bogdanii* (Extended Data Fig. 2c) was supported by shared derived alleles (Extended Data Fig. 2d). Selective sweep analyses (composite likelihood ratio and Tajima's *D*) identified 98.92 Mb of selective sweep regions in the *H. brevisubulatum* genome, encompassing 3,162 protein-coding genes enriched in stress response pathways (Extended Data Fig. 2e,f and Supplementary Data 8). One notable gene, *SOS1*, part of the highly conserved salt resistance signalling pathway[31,32], exhibited pronounced selective sweep signals in I-genome species (five copies in most Old World species and four copies in New World species) and the Xa reference genome (four copies) but remained a single copy in the 20 *H. vulgare* pan-genome accessions (Extended Data Fig. 2g and Supplementary Data 9). These findings underscore the adaptive evolution of *H. brevisubulatum* to stress environments.

Duplication and HGT facilitate saline–alkaline adaptation

In stress screening experiments, *H. brevisubulatum* showed superior tolerance to alkaline salinity compared to other *Hordeum* species (Extended Data Fig. 3a), exhibiting higher survival rates and biomass (Extended Data Fig. 3b,c) under both alkaline (pH ~9.2) and neutral (pH ~7.0) salinity. It also maintained nitrate uptake more effectively than *H. vulgare* under these stress conditions (Extended Data Fig. 3d). Genomic analyses identified several features that may have contributed to its enhanced saline–alkaline stress tolerance.

Duplication of stress-sensing module enhances nitrogen use efficiency for alkali tolerance. Using *H. brevisubulatum* as a reference for the I genome and *H. vulgare* cv. Morex[33] for the H genome, we examined gene copy number variations (gCNVs) across 39 I-genome and 22 H-genome accessions (Supplementary Data 7). Genes expanded in the I genome were enriched notably for GO terms associated with salt and alkali stress adaptation (Supplementary Data 11). Among these, orthologues to wheat *aluminum-activated malate transporter1*[34] and rice H^+*-ATPase*[35] (*TaALMT1* and *OsAHA3*; Supplementary Table 7), typically single-copy genes in *H. vulgare* and *H. marinum*, were duplicated in *H. brevisubulatum*. Calcium-binding EF-hand protein-encoding genes (*CaBPs*) exhibited extensive expansion from two copies in *H. vulgare* to five in *H. marinum* and eight in *H. brevisubulatum* (Fig. 2a and Supplementary Table 7). These eight copies formed tandem repeats within a 0.3 Mb region (Extended Data Fig. 3e). All CaBP copies, except *HbreCaBP.0750*, were markedly upregulated early in the salt and alkali stress treatments, particularly under alkali stress, while *HbreCaBP.0750* expression was downregulated under both stresses (Fig. 2b). To verify their function, we cloned one *CaBP* (*HbreCaBP.0710*) and overexpressed it in *H. vulgare* cv. Golden Promise, which markedly improved alkali tolerance (Fig. 2c), doubling biomass compared to the wild type (WT) under alkali stress (Extended Data Fig. 3f). In addition to increasing biomass under stress conditions, the transgenic barley exhibited an 87% increase in nitrogen uptake and a 68% enhancement in root nitrogen content (Fig. 2d,e). Moreover, soil-cultivated *HbreCaBP.0710* transgenic barley produced up to 24.6% more tillers (Fig. 2f,g) and achieved a 28.7% higher grain yield (Fig. 2h) compared to the WT. These results confirm the positive role of *CaBP*s in alkali stress tolerance. The extensive expansion of *CaBP*s in *H. brevisubulatum* may have contributed to adaptation to alkali environments.

Given *HbreCaBPs*' function in alkali tolerance (Fig. 2c–h), we further screened for gene interactions with HbreCaBP.0710 in *H. brevisubulatum* through yeast two-hybrid (Y2H) assays (Supplementary Table 8), which identified a high-affinity nitrate transporter NRT2 (Extended Data Fig. 3j and Supplementary Note 1). *NRT2* is also present in the gCNV gene sets and has expanded extensively in *H. brevisubulatum* (25 copies) compared to other Poaceae members (*H. vulgare*, 11 copies; *H. marinum*, 19 copies; *T. aestivum*, 16 copies in A-subgenome, 13 in B-subgenome and 16 in D-subgenome; *Zea mays*, 7 copies; *Oryza sativa*, 4 copies), Asteraceae (*Lactuca sativa*, 13 copies; *Cynara cardunculus*, 8 copies; *Artemisia annua*, 11 copies) and Fabaceae (*Medicago truncatula*, 3 copies; *Glycine max*, 7 copies; *Pisum sativum*, 4 copies) (Supplementary Data 12). In Triticeae, *NRT2* duplicates were predominantly located on chromosome 6, spanning approximately 1 Mb at the distal regions of chromosome 6S (Fig. 2i and Extended Data Fig. 3g). It is worth noting that *NRT2* genes were induced exclusively under alkali stress (Extended Data Fig. 3h). Overexpression of one *NRT2* (*HbreNRT2.6420*) in *H. vulgare* cv. Golden Promise enhanced alkali tolerance in transgenic lines (Fig. 2j and Extended Data Fig. 3i), boosting nitrate uptake rate by 24% and enhancing nitrate-nitrogen content by 63% (Fig. 2k,l), consistent with the higher nitrate uptake phenotype of *HbreCaBP.0710* transgenic lines (Fig. 2d,e). These findings highlight the critical role of the CaBP-NRT2 complex in maintaining nitrate uptake and nitrogen content under alkali stress (Fig. 2m), potentially contributing to the adaptation of *H. brevisubulatum* to alkali stress.

Horizontally transferred gene from fungus enhances alkaline–saline tolerance via reactive oxygen species modulation. Reactive oxygen species (ROS) regulation is crucial for plant saline–alkaline tolerance. In *H. brevisubulatum*, ROS levels stabilized after alkali or salt stress, whereas cultivated barley (*H. vulgare*) exhibited excessive ROS accumulation (Extended Data Fig. 4a,b and Supplementary Note 2). Comparative analysis of the three *Hordeum* reference genomes (I, H and Xa) revealed extensive chromosomal inversions and translocations at the distal regions of chromosome 7L (Fig. 3a), including an inversion breakpoint containing four gene duplicates (*HbreFhb7.1*–*HbreFhb7.4*), homologous (>97.8%) to *Fhb7* (ref. 18) (Fig. 3b, Supplementary Fig. 3 and Extended Data Fig. 4c–e). Originally acquired via HGT from the endophytic fungus *Epichloë* to *T. elongatum* and involved in *Fusarium*

https://doi.org/10.1038/s41477-025-01942-w

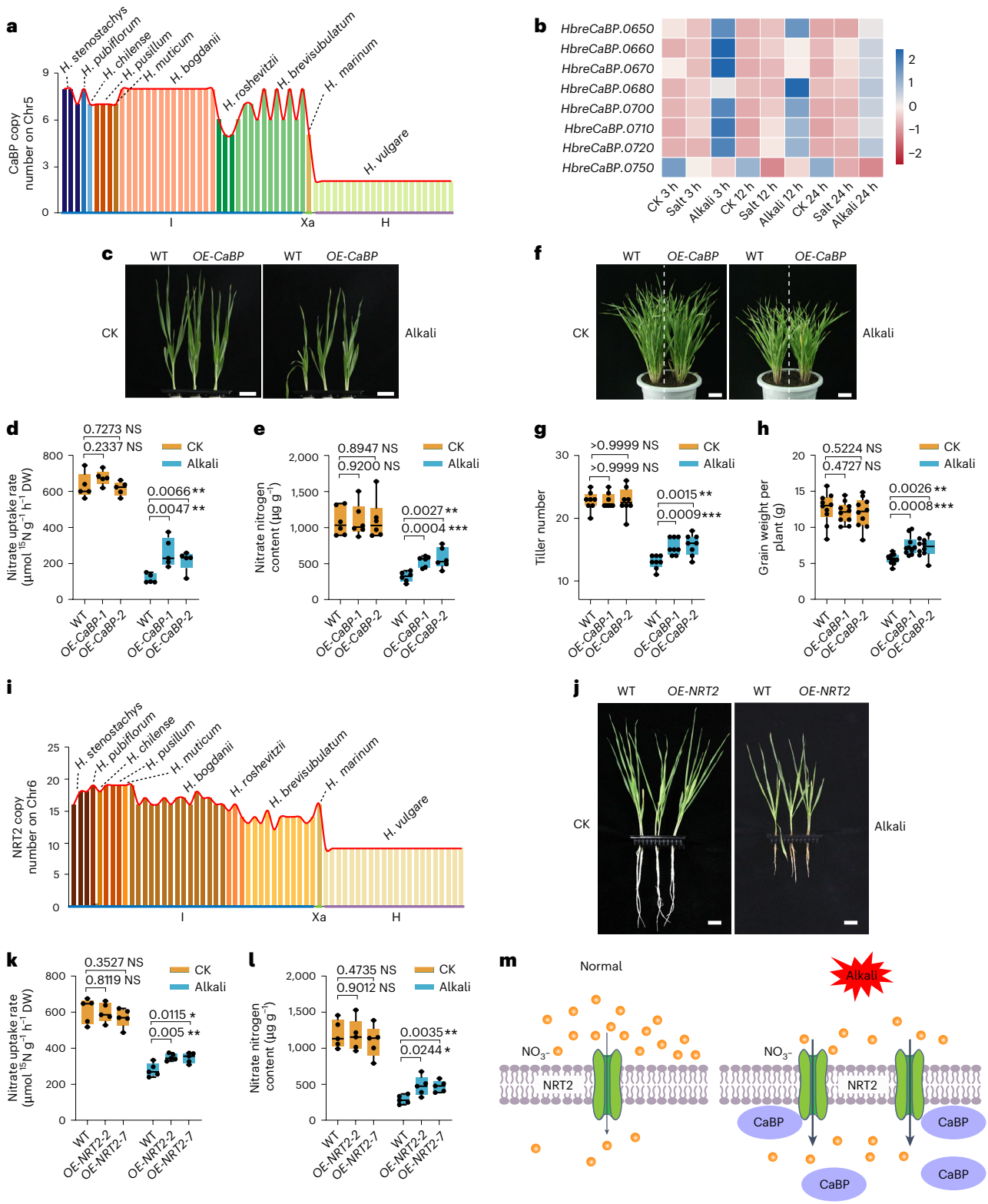

Fig. 2 | Novel CaBP-NRT2 module duplicates enhance alkali tolerance via improvement of NUE. a, The presence of *CaBP* duplicates in the I-genome species, *H. marinum* and *H. vulgare* accessions. **b**, Heat map showing the expression patterns of *HbreCaBPs* in response to alkali and salt stresses in the roots of *H. brevisubulatum*. **c**, Phenotype of *HbreCaBP* transgenic plants under alkali stress. CK, control plants. Scale bars, 3 cm. **d**,**e**, Nitrate uptake rate (**d**) and nitrate nitrogen content (**e**) of *HbreCaBP* transgenic plants under alkali stress for 2 days. **f**, Phenotype of soil-grown *HbreCaBP* transgenic plants under alkali stress for 21 days. Scale bars, 5 cm. **g**,**h**, Comparison of tiller number (**g**) and grain weight per plant (**h**) between *HbreCaBP* transgenic plants and WT under alkali stress. **i**, The presence of *NRT2* duplicates in the I-genome species, *H marinum* and *H. vulgare* accessions. **j**, The phenotype of *HbreNRT2* transgenic plants under alkali stress. Scale bars, 3 cm. **k**,**l**, Nitrate uptake rate (**k**) and nitrate nitrogen content (**l**) of *HbreNRT2* transgenic plants under alkali stress. **m**, A thematic model of stress sensor-responder module CaBP-NRT2. Boxplots show the median, 25th–75th interquartile range (IQR) and minima and maxima (whiskers) with $n = 5$ biological replicates for **d**, **k** and **l**; $n = 6$ for **e**; $n = 8$ for **g**; and $n = 10$ for **h**. Significant differences were calculated using a two-tailed Student's *t*-test (*$P < 0.05$; **$P < 0.01$; ***$P < 0.001$; NS, non-significant).

https://doi.org/10.1038/s41477-025-01942-w

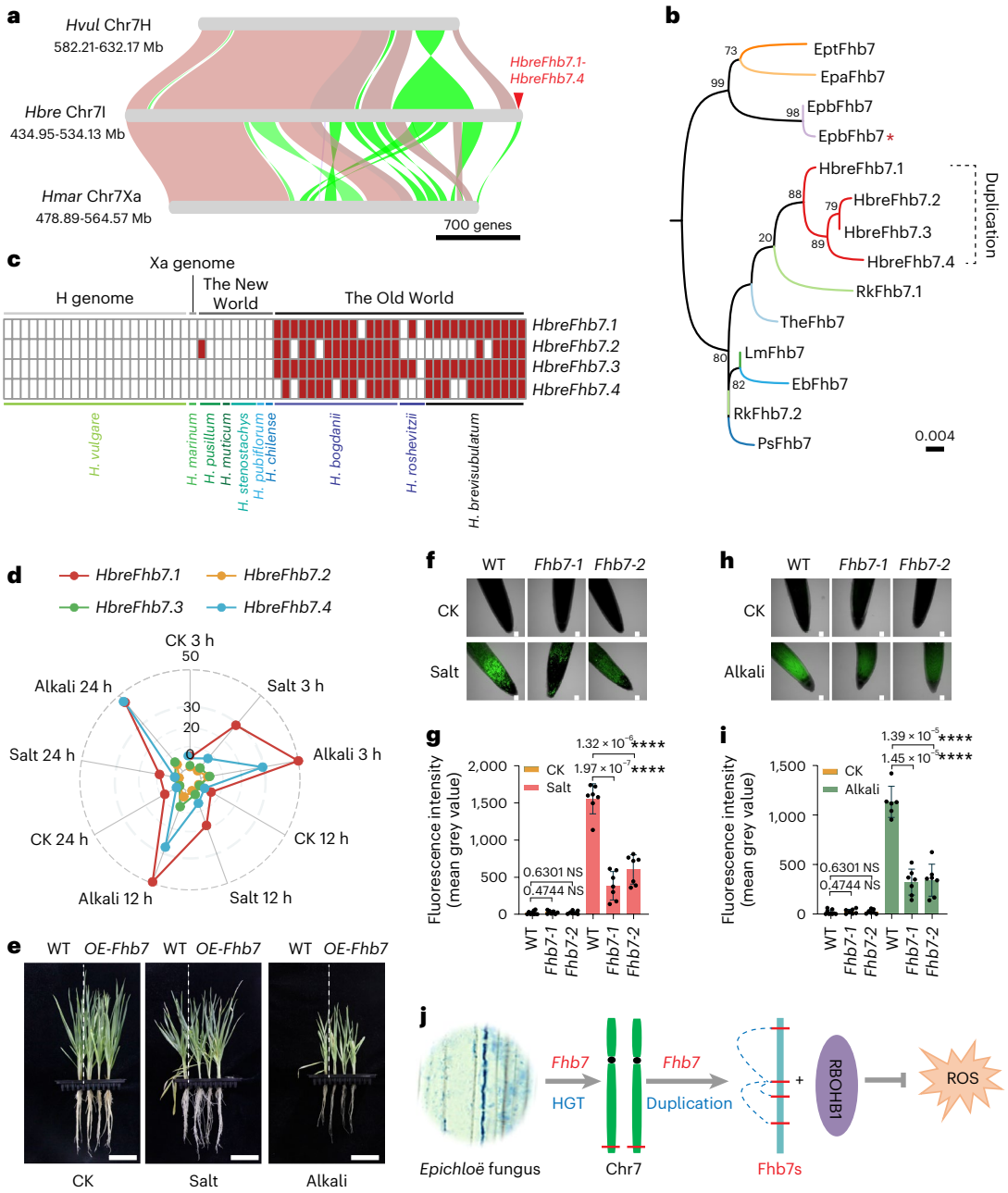

Fig. 3 | HGT and duplication of *HbreFhb7* enhance stress adaptation in *H. brevisubulatum*. **a**, *HbreFhb7* next to the inversion in the ends of chromosome 7L among three *Hordeum* genomes; this figure is shown by gene order. **b**, Phylogenetic relationship between Fhb7 from the reported Triticeae wild species including *H. brevisubulatum* and homologues in *Epichloë* species. The asterisk (*) represents the endophytic fungus *Fhb7* isolated from Old World species *H. bogdanii*. The HGT-derived and duplicated *Fhb7* in *H. brevisubulatum* was labelled with a dashed box. **c**, Distribution of the four copies of *HbreFhb7* among *Hordeum* species. **d**, Radar map indicating expression pattern of *HbreFhb7s* in response to alkali and salt stresses in the roots of *H. brevisubulatum*. **e**, Phenotypes of *HbreFhb7* transgenic plants under alkali and salt stresses. Scale bars, 5 cm. **f**,**h**, Comparison of ROS accumulation in roots of *HbreFhb7* transgenic plants and the WT Golden Promise under salt (**f**) and alkali (**h**) stresses. Scale bars, 100 μm. **g**,**i**, Quantification of the relative fluorescence intensity of the roots stained with H2DCFDA under salt (**g**) and alkali (**i**) stresses. **j**, Work model indicating that HGT and duplication events of *HbreFhb7* innovate saline–alkaline tolerance by suppressing ROS accumulation. The error bars represent mean ± s.d. with $n = 7$ biological replicates for **g** and **i**. Significant differences were calculated using a two-tailed Student's *t*-test (****$P < 0.0001$; NS, non-significant).

head blight resistance[18], *Fhb7* belongs to the *GST* superfamily and has no homologues outside Triticeae (Supplementary Fig. 3, Supplementary Data 13 and Supplementary Note 3). We isolated *Epichloë* strains from *H. bogdanii* seeds and shoots (Extended Data Fig. 4c,d), supporting the proposed HGT event[18]. Moreover, *Fhb7* exhibited clear copy number variations (CNVs) across the *Hordeum* species, preferentially retained in Old World *H. brevisubulatum* and *H. bogdanii* (2–4 copies), with only one copy in New World *H. pusillum* and none in *H. vulgare* or *H. marinum* (Fig. 3c). We found that *HbreFhb7s* had various *cis*-elements involved in abiotic stress response in their promoter regions (Extended Data Fig. 4f), induced by alkali and salt stresses (Fig. 3d). Co-expression analysis linked *HbreFhb7* with key transcription factors (*MYB*, *WKRY*, *ERF* and *bHLH*) and several genes encoding protein kinases (Extended Data Fig. 4g).

Functional validation of *HbreFhb7* was conducted via overexpression of *HbreFhb7.1* (preserved in most *H. brevisubulatum* accessions

and highly induced upon alkali or salt stress) in barley cv. Golden Promise. Transgenic plants showed enhanced biomass under alkali and salt stress (Fig. 3e and Extended Data Fig. 4h) and reduced ROS accumulation (Fig. 3f–i), with no significant differences under control conditions, supporting *HbreFhb7*'s role in maintaining cellular redox homeostasis under alkali and salt stresses. The Y2H assays identified interactions between *HbreFhb7* and several redox-related enzymes, including RBOH, GSTU6, GSTF11 and USP (Supplementary Table 9). We cloned the C-terminals of 10 RBOHs from *H. brevisubulatum*, confirming that HbreRBOHB1 interacted with HbreFhb7 (Extended Data Fig. 4i and Supplementary Note 1). A transient expression assay verified that ROS levels markedly declined when *RBOHB1* was co-expressed with *HbreFhb7* (Extended Data Fig. 4j and Supplementary Note 2). Figure 3j summarizes the genetic origin of *HbreFhb7* and its biological mechanisms in conferring alkali and salt stress tolerance through regulating ROS production.

Potential of the *Hordeum* I genome for wheat improvement

The genetic potential of the *Hordeum* I genome for enhancing wheat stress tolerance was validated through *Tritordeum*[8], a newly synthesized hexaploid species (AABBII) developed by replacing wheat's D subgenome with the *Hordeum* I genome (Fig. 4a). Compared to hexaploid bread wheat 'Chinese Spring' (AABBDD), *Tritordeum* accession HT621 showed substantially improved tolerance to alkali and salt stresses (Fig. 4b and Extended Data Fig. 5a,b). Consistent with the *Hordeum* I genome's inherent adaptability for maintaining nitrogen use efficiency under stress, HT621 exhibited a 47% increase in nitrate uptake rate and a 53% increase in nitrate nitrogen content compared to Chinese Spring under these conditions (Fig. 4c and Extended Data Fig. 5c).

Genomic analysis of HT621 revealed 4,248 homoeologous syntenic triads (1:1:1 ancestral triads) across its three subgenomes (Supplementary Data 14). Gene expression was balanced under control conditions (Fig. 4d and Extended Data Fig. 5d,f). However, under alkali and salt stresses, the I subgenome exhibited a more robust transcriptional response (Extended Data Fig. 5e), with higher expression of stress-responsive genes than the A and B subgenomes (Fig. 4e). Up to 300 differentially expressed genes were identified in the I subgenome, mainly 12 h and 24 h after treatment (Extended Data Fig. 5g), substantially enriching stress-responsive pathways (Extended Data Fig. 5h).

Stress-induced genes unique to the I subgenome (Supplementary Data 15) included those encoding Ca^{2+} signalling sensors (*CaBP.0650* and *CaBP.0710*); transcription factors (*WRKY*s); Na^+-exclusion protein (*SOS1*); transporters for phosphate, iron and sugar; and genes related to abscisic acid signalling, osmotic stress and ROS regulation, which were particularly responsive under alkali stress (Fig. 4f). Key nitrogen metabolic pathway genes, including *NRT2* (high-affinity nitrate transporter), *NR1.1* (nitrate reductase), *GS1.1* (glutamine synthetase), *NADH-GOGAT* (NADH-dependent glutamate synthase) and *Fd-GOGAT* (ferredoxin-dependent glutamate synthase), exhibited higher expression in the I subgenome than in the A and B subgenomes (Fig. 4g). These genetic features likely underpin the enhanced nitrate uptake and nitrogen assimilation in *Tritordeum*, contributing to its improved salt and alkali tolerance. A model illustrating these pathways are presented in Fig. 4h.

Discussion

In this Article, we assembled a high-quality chromosome-scale *H. brevisubulatum* genome that can be used as a reference genome for I-genome species. Through comprehensive genomic, evolutionary and genetic analyses, we established a foundation for exploring the evolutionary relationships and adaptive traits of the *Hordeum* I-genome species. These species, recognized as important CWRs, harbour valuable genetic diversity that can enhance crop resilience and improve adaptive traits in breeding programs[9]. It is worth noting that *H. brevisubulatum* is a facultative halophyte with superior salt tolerance despite lacking specialized salt-exclusion structures such as salt glands[12] (https://ehaloph.uc.pt/). Consistent with earlier research[11], we found that *H. brevisubulatum* exhibited greater tolerance to neutral salts than Xa- and H-genome species (*H. marinum* and *H. vulgare*, respectively) and a unique ability to tolerate alkaline salts (alkali), underscoring its evolution of genetic strategies for both alkali and salt stress tolerance.

Adaptation to salt and alkali stress in the *Hordeum* I genome

Structural variations substantially contribute to speciation and genome evolution[36]. The *H. brevisubulatum* genome revealed notable chromosome inversions, translocation and gCNVs compared to the Xa-genome (*H. marinum*) and H-genome (*H. vulgare*) reference genomes. These structural variations, particularly the extensive expansion of stress-related genes, align with observations in other halophytic species, such as *Achnatherum splendens*[37] and *Spartina alterniflora*[38], and likely drive adaptation to harsh environments.

Among these structural variations, gCNVs have emerged as key contributors to plant evolution and adaptation[19,39]. Unique gCNVs in the *H. brevisubulatum* genome were enriched with GO terms related to stress adaptation, including several stress-responsive and transporter-encoding genes. The *SOS1* gene, a well-characterized locus essential for salt tolerance and Na^+ exclusion within the Salt Overly Sensitive (SOS) pathway[40], has expanded to five copies in *H. brevisubulatum*, compared to one copy in *H. vulgare* and four copies in *H. marinum*. In the halophytic *Arabidopsis thaliana* relative *Thellungiella salsuginea*, *SOS1* is a key determinant of halophytism[41]. Supporting its role in tolerance, studies have shown that mutations in *SOS1* in the halophytic grass *H. marinum* lead to diminished salt tolerance[42]. The expansion of *SOS1* in *H. brevisubulatum* likely contributes to its enhanced salt tolerance, reinforcing the critical role of this gene in plant adaptation to saline environments. Similarly, genes pivotal for alkali tolerance, such as *AHA3* (regulating H^+ flux and pH gradients in saline–alkaline stress[35,43]) and *ALMT1* (a malate-GABA (gamma-aminobutyric acid) transporter conferring alkaline tolerance in wheat[34]), were duplicated in the *H. brevisubulatum* genome. These duplications, alongside the expansion of other stress-related genes, may help explain the superior salt and alkali tolerance observed in I-genome species compared to Xa- and H-genome species. Unlike other sequenced *Hordeum* species, which are annuals, *H. brevisubulatum* is perennial. This difference, coupled with the gCNV-mediated expansion of stress-tolerance genes such as *SOS1*, *AHA3* and *ALMT1*, suggests broader adaptive traits beyond salt and alkali tolerance, including life history strategies. These findings underscore the importance of continued explorations of *H. brevisubulatum* to understand its unique genetic and adaptive strategies.

Salt and alkali tolerance mechanisms in *H. brevisubulatum*

While the molecular mechanisms of salt tolerance in plants are well studied[44], the understanding of alkali tolerance mechanisms remains limited[14]. Calcium signalling plays a crucial role in salt tolerance; however, how alkali stress signals are detected is not fully characterized. One key player is *CaBP*, an EF-hand Ca^{2+}-binding protein that senses stress signals by binding Ca^{2+} and transducing them to downstream genes[15]. Studies have shown that *CaBPs* can act as negative or positive regulators under saline–alkaline stress[16,45]. Leveraging the *H. brevisubulatum* reference genome, we identified an expansion of *HbreCaBP*. Experimental validation revealed that these proteins are induced under high alkali stress and contribute positively to alkali tolerance in transgenic barley, suggesting their role as Ca^{2+} sensors and regulators. This expansion may enhance stress responses, indicating a potential target for breeding alkali-tolerant crops. Further studies are needed to explore allelic variations and their contributions to this adaptive trait.

Our findings also revealed that *H. brevisubulatum* maintains a higher nitrate uptake rate under alkali or salt stress than *H. vulgare*, indicating this is a critical adaptive strategy. This capability is underpinned by a dramatic expansion of the high-affinity nitrate

https://doi.org/10.1038/s41477-025-01942-w

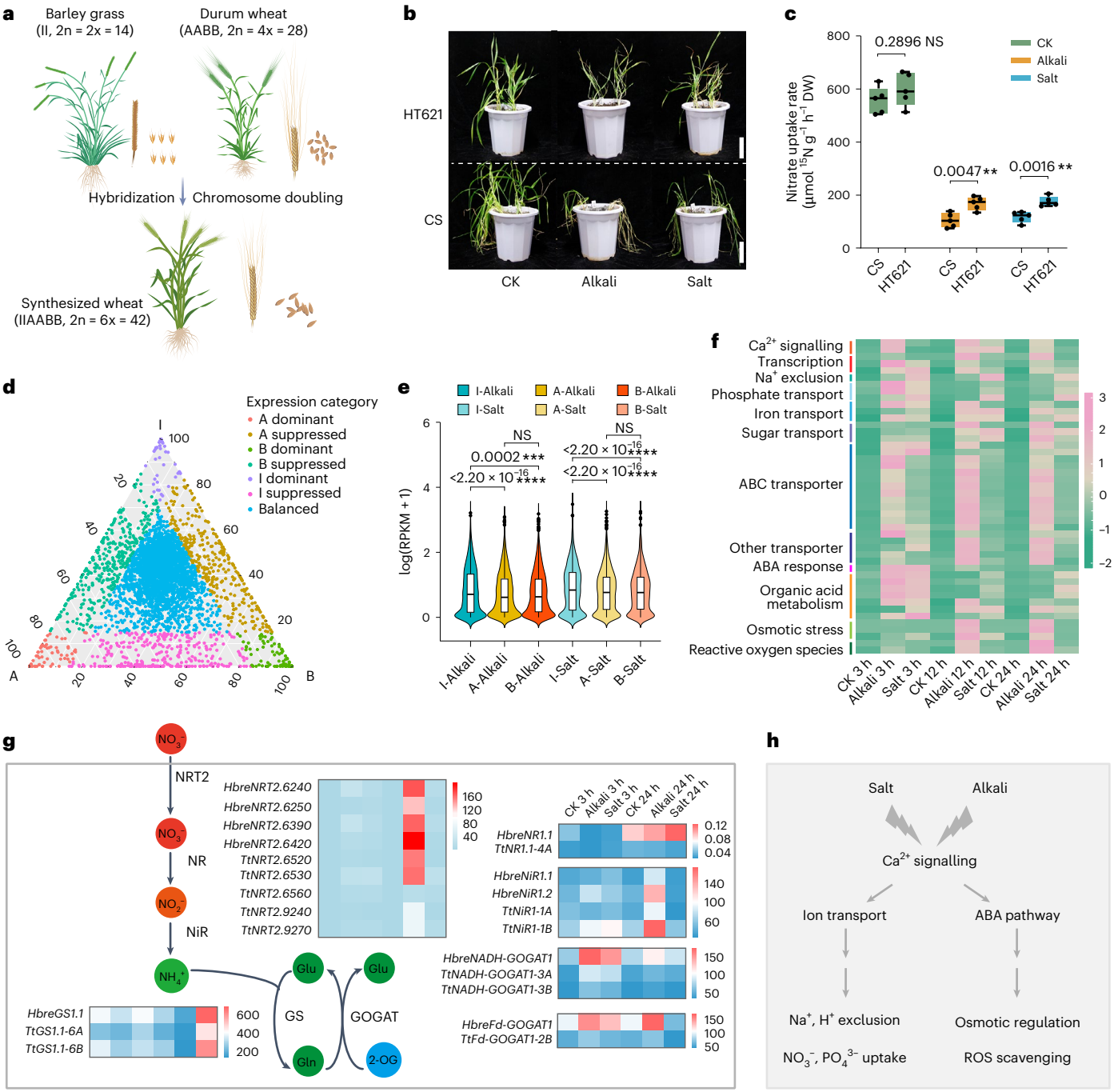

Fig. 4 | The *Hordeum* I genome holds great potential for improving stress tolerance. a, Graphic illustration of the creation of *Tritordeum* (AABBII). **b**, Comparison of phenotypic changes between *Tritordeum* HT621 and Chinese Spring under salt or alkali stress. Scale bars, 10 cm. **c**, Nitrate uptake rate of HT621 and Chinese Spring under salt or alkali stress. **d**, Ternary plot showing the relative expression levels of ancestral triads in *Tritordeum* HT621 roots. Each dot represents a gene triad with an A, B and I coordinate; balanced triads are represented by blue dots in the centre. **e**, Violin plots of the expression of ancestral triads in the A, B and I subgenomes of *Tritordeum* HT621 in response to alkali and salt stresses in roots. The significance of the difference is determined using a Kruskal–Wallis test (***$P < 0.001$; ****$P < 0.0001$; NS, non-significant). **f**, Heat map of the specific genes or duplicates in the I subgenome with markedly up-regulated expression but no homoeologues in the A and B subgenome of HT621. **g**, The nitrogen metabolic pathway and the expression of representative genes in the subgenomes of HT621 under alkali and salt stresses in roots. **h**, Thematic model illustrating the effect of substituting the D subgenome with the *Hordeum* I genome in improving *Tritordeum* alkali or salt stresses tolerance. Boxplots show the median, 25th–75th IQR, and minima and maxima (whiskers) with $n = 5$ biological replicates for **c**. Significant differences were calculated using a two-tailed Student's *t*-test (**$P < 0.01$; NS, non-significant).

transporter-encoding gene *NRT2*, which has 25 copies in *H. brevisubulatum*—the highest among Poaceae species with sequenced genomes. *NRT2* genes are known to facilitate nitrate uptake under low-nitrogen conditions[46–48], but their interaction with the expanded *CaBP* suggests a sensor-responder module that contributes to alkali tolerance. This module likely helps mitigate the nutritional imbalance caused by alkali stress, strengthening the plant's resilience. Further research is required to elucidate the signal transduction and activation between *CaBP*s and *NRT2* under stress. Drawing parallels with studies on alkali-tolerant legumes such as *Sesbania cannabina*,

which uses expanded phosphorus-transporter genes to maintain nutrient uptake[49], we propose that *H. brevisubulatum* uses the expanded *CaBP-NRT2* module similarly.

Another important finding is the retention and expansion of HGT-derived *Fhb7* genes in *H. brevisubulatum*. Originally identified as a product of a fungus-to-plant HGT event in *T. elongatum*[18], *Fhb7* has since been observed in other Triticeae species[50]. Symbiotic associations between endophytic *Epichloë* fungi and Pooideae species likely serve as the basis for the transfer of *Fhb7* and other HGT-derived genes[51,52]. We isolated the *Epichloë bromicola* strain from Old World *H. bogdanii*, supporting the occurrence of the HGT event. The presence of *Fhb7* in multiple Triticeae species suggests either a shared ancestral HGT event or multiple independent occurrences. Remarkably, *H. brevisubulatum* has expanded *Fhb7* from one to four copies, distinguishing it from other species. These genes are more abundant in Old World I-genome species, indicating dynamic changes in structurally active genomic regions, consistent with the positioning of *Fhb7* near a structural inversion in our assembled genome. Beyond its known role in *Fusarium* head blight tolerance in wheat[18], our transgenic studies revealed that *HbreFhb7* potentially contributes to alkali and salt tolerance by reducing ROS accumulation. The conservation and expansion of *HbreFhb7* likely play a crucial role in *H. brevisubulatum*'s adaptation to saline–alkaline environments.

Genetic potential of I-genome species for crop breeding

The superior abiotic stress resilience of I-genome species offers immense potential for enhancing barley and wheat breeding programs. Several I-genome species have already been used in traditional hybridization efforts, improving agronomic performance in modern wheat and barley varieties[8,9]. The *H. brevisubulatum* genome sequence, combined with insights into its adaptive strategies and alkaline–saline tolerance mechanisms, provides a valuable resource for optimizing the use of I-genome species in crop improvement.

Through phenotypic evaluations of hexaploid *Tritordeum* (AABBII) under stress conditions, we demonstrated that substituting the D-subgenome with the I-subgenome substantially enhanced alkaline–saline tolerance. It is worth noting that the hexaploid *Tritordeum* exhibited higher nitrate uptake rates and nitrogen content under alkali and salt stress, supporting the role of the expanded *CaBP-NRT2* module as a critical molecular mechanism underlying I-genome species' stress adaptation. Moreover, we found that I-subgenome genes in the synthesized hexaploid showed enhanced transcriptional responsiveness to stress conditions. This transcriptional regulation—observed under stress conditions but not in the control—highlights an additional evolutionary strategy, complementing genomic structural variations, used by I-genome species for stress adaptation.

Our findings highlight the immense potential of harnessing the genetic diversity of I-genome species into breeding programs through transgenic and crossbreeding approaches to develop stress-resilient crops. Alternatively, de novo domestication of I-genome species with agronomic potential presents a promising avenue for future crop development[53]. By decoding the *Hordeum* I genome, we have created a strong foundation for leveraging these genetic resources, which are crucial for advancing sustainable agriculture and ensuring food security, particularly for developing crops that can thrive in soils affected by salt or alkali toxicity. Our study paves the way for establishing an advanced crop breeding platform to improve wheat and barley resilience and productivity.

Methods

Plant materials and genome sequencing

H. brevisubulatum accession PI531775 was sourced from the US NPGS and cultivated in a greenhouse under a 16 h light/8 h dark cycle at 24 °C and 16 °C, respectively. Genome size (~3.65–3.77 Gb) and diploidy were confirmed via flow cytometry using *Z. mays* cv. B73 (~2.3 Gb) and *H. vulgare* cv. Morex (~5.04 Gb) as standards. DNA was extracted from 3-week-old leaves using a DNAsecure Plant Kit (TIANGEN). Seven ~15 kb DNA-insert libraries were sequenced on a PacBio SEQUEL II platform at Novogene, generating 162.12 Gb HiFi reads (~45× coverage). In addition, 350 bp DNA-insert libraries were sequenced on an Illumina HiSeq platform (150PE) at BioMarker, generating 579.78 Gb paired-end reads (~161× coverage). Five Hi-C libraries were constructed from cross-linked chromatins using a standard Hi-C protocol and sequenced on the Illumina HiSeq platform at BioMarker, yielding 568.61 Gb Hi-C reads (~158× coverage).

Genome assembly and annotation

Genome size estimation. Genome size was estimated using *K*-mer distribution analysis with Kmc v3.2.1 (ref. 54) and genomescope v1.0.0 (https://github.com/schatzlab/genomescope/). The *K*-mer value used for the genome survey was 21.

Genome assembly. Contig-level assembly was performed using hifiasm v0.14.0 (ref. 55) with HiFi reads as input, applying default parameters. Read error correction used a Falcon-like algorithm integrated into the hifiasm pipeline. Hi-C scaffolding was conducted by aligning Hi-C sequencing data to the assembled genome using Juice_tools v1.8.9 (ref. 56), followed by chromosome construction with 3D-DNA v180419 (ref. 57).

Gene annotation. Gene structures were predicted using the GETA v2.4.5 pipeline (https://github.com/chenlianfu/geta), integrating ab initio gene prediction, homologous proteins and transcriptome data using Augustus v2.5.5 (ref. 58), Trimmomatic v0.40 (ref. 59), HiSAT2 v2.2.1 (ref. 60) and genewise v2.4.1 (https://www.ebi.ac.uk/~birney/wise2/).

Repetitive sequences were identified and masked to reduce background noise from frequently duplicated transposable elements. The RNA-sequencing (RNA-seq) data underwent trimming with Trimmomatic before alignment to the reference genomes using HISAT2. Subsequently, the GETA pipeline calculated coverage thresholds specific to each alignment region based on the sequencing depth. Transcripts falling below the coverage cutoff were filtered out to prioritize reliable introns and optimize transcripts. The remaining high-quality transcripts were subjected to open reading frame (ORF) prediction in TransDecoder v 5.5.0 (https://github.com/TransDecoder/TransDecoder). Guided by earlier predicted intron and exon structures, the gene models underwent iterative training using Augustus v2.5.5 (ref. 58) to achieve the best score. In addition, homologous proteins from *A. thaliana*, *O. sativa*, *Actinidia chinensis* from Phytozome v12 (https://phytozome.jgi.doe.gov/), *Brachypodium distachyon*, *Sorghum bicolor* and *Z. mays* from EnsemblPlants release-50, and previously published barley[27] and wheat[61] proteins were used for further protein identification via Genewise v2.4.1.

Repeat annotation. Genome-wide transposable element annotation was conducted using EDTA v2.0.0 (ref. 62). Transposable elements, including LTR-RTs and DNA transposons, were identified in *H. brevisubulatum*, *H. marinum* and *H. vulgare*. RepeatMasker v4.1.5 (ref. 63) was used to align the genome assemblies of these species against the clariTeRep repeat library in CLARI-TE (https://github.com/jdaron/CLARI-TE), enabling LTR subfamily classification. The LTR assembly index was evaluated for *H. brevisubulatum*, *H. marinum*, *H. vulgare*, *T. elongatum* and *Dasypyrum villosum* by integrating results from LTR_Finder v1.07 (ref. 64) and LTR_harvest v1.6.1 (ref. 65) using LTR_retriever v2.9.0 (ref. 66). To infer centromere positions, *Gypsy* retrotransposons *Cereba* and *Quinta*, enriched in centromeric regions of *Triticum* species[61,67], were analysed[42,68]. Putative centromeric regions in *H. brevisubulatum* were identified based on the enrichment of *RLG_famc8.3* (*Cereba*), *RLG_famc8.1* (*Quinta*) and *RLG_famc8.2* (*Quinta*), following methodologies established in previous studies[42,68].

BUSCO assessment. Genome completeness was assessed using BUSCO analysis. The completeness evaluation for *H. brevisubulatum*, *H. marinum*, *H. vulgare*, *T. elongatum* and *D. villosum* was performed using compleasm v0.2.5 (ref. 69) with the Poales_odb10 database.

Comparative genomics and genome evolution analysis

Phylogenetic tree construction. Orthologous gene families across 15 species—*H. brevisubulatum*, *H. marinum*[42], *H. vulgare* cv. Morex[33], *H. vulgare* B1K0412[27], *T. aestivum*[61] (subgenomes A, B and D), *A. speltoides*[70], *T. urartu*[71], *A. tauschii*[72], *T. elongatum*[18], *S. cereale*[73], *A. sativa*[74] (subgenomes A, C and D), *P. tenuiflora*[75], *B. distachyon*[76], *O. sativa*[77] and *Ananas comosus*[78]—were identified using OrthoFinder v2.5.4 (ref. 79) after excluding sequences shorter than 100 amino acids. All-vs-all Blastp v2.2.31 for the 268 identified single-copy genes identified only 10 gene pairs with minimal redundancy (4%) with high sequence identity (>50%) among 11 unique genes, which was deemed negligible for species phylogeny.

Three approaches were used to construct the species tree[80,81]. First, each coding sequences (CDS) of the 268 single-copy homologous genes was aligned using MUSCLE v3.8.31 (ref. 82) and trimmed with trimAL v1.2 (ref. 83) ('-automated1'). IQTREE2 v2.1.4-beta (ref. 84) was used to construct 268 trees with self-estimated best substitution models, and a coalescent-based species tree was generated with Astral v 5.7.8 (ref. 85). Second, concatenated protein sequences from OrthoFinder were aligned using MUSCLE v3.8.31, converted to CDS alignments using PAL2NAL v14 (http://www.bork.embl.de/pal2nal/index.cgi#RunP2N) and trimmed using trimAL v1.2 ('-automated1'). ModelTest-NG v 0.1.6 (ref. 86) selected the best-fit substitution model (GTR + I + G4) for maximum likelihood tree construction using PhyML v3.088 (ref. 87). Third, Bayesian phylogenies were constructed with MrBayes v3.2.7a using the general time-reversible (GTR) model with six substitution types (nst=6) and invgamma rate distribution, running two independent Markov chain Monte Carlo chains every 100 trees for 200,000 generations. Convergence was confirmed with standard deviations below 0.05 and effective sample size (ESS) above 200. The verified maximum likelihood phylogenetic tree was visualized using iTOL (https://itol.embl.de/).

Phylogenomic dating and branch length analysis were conducted using MCMCtree in PAML v4.9 (https://github.com/abacus-gene/paml), using an auto-correlated JC69 substitution model with uniform priors on relative node times. Calibration times were derived from known species divergence dat in Timetree (http://www.timetree.org/).

Gene family analysis. Gene family expansions and contractions were detected using CAFE v4.2.1 (ref. 88) with a significance threshold ($P < 0.05$). Orthologous families identified via OrthoFinder were filtered to exclude those with abnormal gene counts. Filtered families and the ultrametric tree were input into CAFE following the tutorial (https://hahnlab.github.io/CAFE/src_docs/html/index.html), optimizing the birth and death rate parameter (λ) across all families with the '-s' and '-t' parameter. Gene family identification was conducted using Hmmer v3.3.2 (ref. 89) and Blastp. Model HMM files from the Pfam database (v35.0) were used to detect family-specific protein sequences ($e < 0.01$). Homologous protein sequences were identified with Blastp ($e < 1 \times 10^{-10}$). Phylogenetic trees were constructed with RAxML-NG v1.2.2 (ref. 90), while candidate gene family proteins were validated against Pfam and National Center for Biotechnology Information Conserved Domains databases. Transcription factor families were identified using PlantTFDB (http://planttfdb.gao-lab.org/prediction.php). Predicted transcription factors were manually validated by confirming associated domains in the InterPro database (https://www.ebi.ac.uk/interpro/).

Genome collinearity and duplication analysis. Structural variations among the genomes of *H. brevisubulatum, H. marinum* and *H. vulgare* cv. Morex were analysed using GeneSpace v1.1.4 (ref. 91), which leverages orthogroup identification tools such as OrthoFinder, MCScanX and Diamond v 2.1.8 to define syntenic regions[92]. The *H. vulgare* cv. Morex genome was used as the reference, with inversions highlighted in green. Plots were generated based on both physical and gene rank order. Collinear gene pairs identified by MCScanX v1.0.0 were further processed to calculate whole-genome 4dtv and synonymous substitution values using wgd v1.1.2 (ref. 93). Micro-synteny analyses of *HbreCaBP* and *HbreNRT2* genes between species were performed with MCScanX (default parameters) and visualized using jcvi v1.2.10 (https://github.com/tanghaibao/jcvi). Gene duplications in *H. brevisubulatum*, *H. marinum* and *H. vulgare* cv. Morex were classified into five types—whole-genome duplication (WGD), tandem duplication, proximal duplication, transposed duplication and dispersed duplication—using DupGen_finder v1 (ref. 94) with default settings.

Resequencing and population analysis

Resequencing reads mapping and variant calling. Thirty-eight I-genome accessions from populations across China (Nei Monggol, Xinjiang, Gansu, Qinghai and Tibet provinces), Kazakhstan, Iran, South Africa, the United States, Peru, Uruguay and Argentina were identified as diploids using flow cytometry, with *H. brevisubulatum* PI531775 or *Z. mays* cv. B73 as the reference standard (Supplementary Data 7). Leaves were collected, and DNA libraries were constructed using a DNAsecure Plant Kit (TIANGEN). Sequencing was performed on the Illumina HiSeq-4000 platform in 150 bp paired-end mode. In addition, raw resequencing data for 22 H-genome accessions and 1 I-genome species were obtained (Supplementary Data 7). Quality control of raw sequencing reads was carried out using FastQC v0.12.1 (ref. 95), followed by adapter and low-quality read trimming using Trimmomatic v0.40 (ref. 59). Clean reads, with an average genome coverage depth of 16.3× (Supplementary Data 7), were aligned to the *H. brevisubulatum* genome using a modified Burrows-Wheeler Aligner (BWA) program from the Sentieon package (v202112.02). The Binary Alignment/Map format (BAM) files underwent an accelerated Genome Analysis Toolkit (GATK)-compliant pipeline, adhering to the 'Broad Institute Best Practices Pipeline'. Quality control metrics included MeanQualityByCycle (MQ > 30.0), QualDistribution (QD > 2.0), GCBias, AlignmentStat and InsertSizeMetricAlgo. Duplicates were identified and removed using LocusCollector and the Dedup algorithm. Uniquely mapped reads with mapping quality >30 were selected (via samtools) and processed with IndelRealigner for accurate small indel detection (1–10 bp). Base quality recalibration was performed using QualCal. Variants were called using the HaplotypeCaller algorithm to identify SNPs and indels, with joint calling performed using GVCFtyper. Variants with low depths, high repetition or more than 15% missing data were filtered from the raw SNP Variant Call Format (VCF) file using VCFtools v0.1.16 (ref. 96) with the following parameters: minDP = 4, minQ = 30, max-missing = 0.85, mac = 4, max-alleles = 2 and min-alleles = 2. Further filtering of SNPs was performed using BCFtools v 1.19 (ref. 97) with the parameters '-e GT == 'het' & DP < 15'. Linkage disequilibrium pruning was conducted with Plink v 1.9.0 using the parameters maf = 0.05 indep = 50 5 2. In total, 810,571 SNPs from single-copy genes were extracted to reconstruct phylogenetic relationships among the 61 accessions. In addition, 1,595,091 SNPs within the CDS region of genes from these accessions were selected for further analysis.

Phylogeny analysis. The SNP VCF file was converted into a DNA sequence alignment file using a custom Perl script. ModelTest-NG v 0.1.6 (ref. 86) was used to identify the best-fit nucleotide substitution model 'GTRGAMMAX'. Maximum likelihood tree was constructed using RAxML-NG v1.2.2, and phylogenetic tree was visualized with iTOL v7.

PCA. VCFtools was used to convert the VCF file into PLINK format, and PCA was conducted using GCTA v1.94.1 (ref. 98). The top three

principal components were visualized and retained for further population structure analysis.

Population genetic structure. Population structure (61 accessions) was inferred using Admixture v1.3.0 (ref. 99) with ancestral population sizes set from $K = 2$ to $K = 9$. The optimal structure was determined at $K = 5$, with the lowest cross-validation error (0.25).

Genetic diversity and introgression estimation. Genome-wide Tajima's D and nucleotide diversity ($\theta\pi$) were calculated using VCFtools with a 50 kb sliding window. Composite likelihood ratio values for 50 kb windows were computed using SweeD v3.3.1 (ref. 100). Gene flow was modeled using TreeMix v 1.13 (ref. 101) with the following parameters: -se, –bootstrap and -k set to 1,000. The number of migration edges (-m) ranged from 1 to 10, with three iterations of each. OptM v0.1.8 (ref. 102) was used to determine the optimal number of migration edges. Introgression was further analysed using Patterson's D-statistic (ABBA-BABA test), implemented in Dsuite v 0.5 (ref. 103).

Population CNVs

Population CNVs were identified using popCNV v1.1.0 (https://github.com/sc-zhang/popCNV), which estimates gene copy number based on sequencing depth and guanine-cytosine (GC) content correction. Sequencing depth was calculated using Mosdepth v0.3.3 (ref. 104) with a 1 kb window size. Population CNVs were identified for the 39 I-genome accessions using *H. brevisubulatum* as the reference genome and for the 22 H-genome accessions using *H. vulgare* cv. Morex[33] as the reference genome. Gene clustering into orthologous groups for *H. brevisubulatum*, *H. vulgare* cv. Morex[33] and *H. marinum*[42] was performed using OrthoFinder. The number of genes in each orthologous group from the I-, Xa- and H-genome accessions were counted to infer CNVs. Candidate gCNVs for 18 H-genome accessions were further validated using Blastn v2.2.31. In cases of discrepancies, Blastn results were prioritized. CNVs for candidate genes were visualized using heat maps generated in the pheatmap package v1.0.12 in R.

Transcriptome sequencing

H. brevisubulatum and *Tritordeum* seedlings were grown hydroponically in 1/4 Hoagland solution (pH 5.8) under controlled conditions (16 h light at 24 °C, 8 h dark at 16 °C) for 2 weeks. Stress treatments involved exposure to either 200 mM NaCl (pH 5.8) or 200 mM $NaHCO_3$ (pH 9.0), with the solution refreshed every 2 days to maintain pH. Roots were collected at ZT6 (3 h after stress), ZT15 (12 h after stress) and ZT6 day 2 (24 h after stress). Total RNA was extracted using an RNAprep Pure kit (Tiangen) with three biological replicates per time point. RNA-seq libraries (350 bp inserts) were prepared and sequenced using Illumina NovaSeq in 150 nt paired-end mode, generating ~6 Gb of raw reads per sample. For *Tritordeum* (AABBII), reads were aligned to a concatenated genome combining the AABB genome of *Triticum turgidum* cv. Svevo[105] and the II genome of *H. brevisubulatum* using STAR v2.7.10 (ref. 106). Low-quality reads were filtered out, and uniquely mapped reads were used to create count matrixes with featureCounts v2.0.4 (ref. 107), normalized to reads per kilobase per million mapped reads (RPKM) via a customized Perl script. Differential expression was conducted using edgeR v4.4.2 with >2-fold change and Benjamini–Hochberg false discovery rate < 0.01. Heat maps were created using the pheatmap package v1.0.12. GO enrichment analysis was performed with the topGO package v2.58.0 and visualized using ggplot2 v3.4.4. Correlation networks were constructed using the weighted correlation network analysis package v1.61 (ref. 108).

Expression bias of *Tritordeum* subgenomes

Homologous gene expression bias in hexaploid *Tritordeum* was analysed following previous methodologies[109] with slight modifications. In total, 4,248 triads of homologous genes were identified using Blast v2.2.31 and MCSanX v1.0.0, representing 1:1:1 correspondences among the three subgenomes and referred to as ancestral triads. Gene expression levels were normalized by calculating each homologue's contribution to total expression within its triad. Based on a threshold of 0.15, each homologous gene pair was classified into one of three expression types: dominant, suppressed or balanced. A ternary plot illustrating subgenomic contributions was generated using the ggtern package v3.4.2 in R.

Salt and alkali treatment

H. brevisubulatum, *H. vulgare* and barley transgenic lines were germinated on wet filter paper before salt and alkali treatment via hydroponic cultivation. After approximately 3 days, seedlings were transferred to 1/4 Hoagland solution (pH 5.8) and grown under controlled conditions (16 h light at 24 °C, 8 h dark at 16 °C). Seedlings of *H. vulgare* were grown for 2 weeks, while *H. brevisubulatum* were grown for 3 weeks, until they reached the three-leaf stage. Treatments involved exposing seedlings to 200 mM NaCl (pH 5.8) or 100 mM $NaHCO_3$ (pH 9.0), with the solution refreshed every 2 days to maintain pH. After 7 days of treatment, plants were photographed, and shoot and root fresh weights were measured. For ^{15}N uptake analysis, seedlings cultured for 2 weeks were subjected to stress treatments with 100 mM NaCl or 50 mM $NaHCO_3$, as described above. Following this, seedlings were treated with $K^{15}NO_3$ for 30 min, rinsed with 0.1 mM $CaSO_4$ solution and deionized water, and dried at 70 °C for 3 days. The dried samples were ground into powder, and the ^{15}N content was measured using an isotope ratio mass spectrometer with five biological replicates. The nitrate uptake rate was defined as the amount of ^{15}N absorbed per unit weight of seedling per unit time, calculated by dividing the total ^{15}N content (μmol ^{15}N) of the whole plant by the seedling's dry weight (g DW) over a 3 h period, following established methods[110,111].

Phenotypic evaluations were conducted on *H. brevisubulatum*, *H. marinum* (PI 200341 from NPGS), *Hordeum murinum* (PI 266198 from NPGS), *H. vulgare* (Golden Promise), *Tritordeum* (HT621), bread wheat (Chinese Spring) and *HbreCaBP* transgenic lines. Seeds were sterilized in 70% ethanol for 30 s, washed three times with distilled water, shaken in 10% bleach solution for 15 min and washed thoroughly with distilled water 8 to 10 times. Seedlings were grown in a controlled greenhouse under long-day conditions (16 h light at 24 °C, 8 h dark at 16 °C). Salt (NaCl) and mixed alkali ($NaHCO_3$:Na_2CO_3 = 5:1, pH 9.2) treatments were applied to soil-grown plants at the third-leaf stage, gradually increasing from 100 mM to 300 mM. After 21 days of treatment, plants were photographed, and shoot and root fresh weights were measured. For transgenic and WT plants, 150 mM mixed alkali treatments were applied for 21 days. Control plants were grown under normal conditions without stress treatments. Phenotypic data, including tiller number and grain yield, were recorded.

Transgenic plant validation

The coding sequences of *HbreCaBP*, *HbreNRT2* and *HbreFhb7* (Supplementary Data 16) were cloned into the pCAMBIA1300 vector under their respective native promoters and terminators. Barley transformation was conducted following a previously published protocol[112] with minor modifications. Briefly, immature embryos from the barley cv. Golden Promise were isolated and incubated with *Agrobacterium* for 10 min. Co-cultivation was performed for 2 days on CM medium (1/10 Murashige and Skoog (MS) medium plus 10 g l^{-1} glucose, 100 μM acetosyringone, and 3.5 g l^{-1} phytagel). After removing embryo axes, scutella were cultured on the first selection medium (MS medium plus myoinositol 0.35 g l^{-1}, 0.69 g l^{-1} proline, 1 mg l^{-1} thiamine HCl, 2.5 mg l^{-1} dicamba, 1 g l^{-1} casein hydrolysate, 10 mg l^{-1} hygromycin B, 160 mg l^{-1} timentin, 1 g l^{-1} 2-(*N*-morpholino) ethanesulfonic acid and 3.5 g l^{-1} phytagel). After 2 weeks, tissues were transferred to the second selection medium, identical to the first but containing 20 mg l^{-1} hygromycin B. Three weeks later, embryonic calli were cultured on

DM medium (first selection medium supplemented with 2.5 mg l^{-1} $CuSO_4{\cdot}5H_2O$, 1 mg l^{-1} kinetin, 0.5 mg l^{-1} 6-benzylaminopurine and 0.05 mg l^{-1} 1-naphthaleneacetic acid) at 25 °C under light conditions to induce differentiation. Regenerated shoots were transferred to RT medium (1/2 MS medium with 1 mg l^{-1} indole butyric acid) and subsequently transplanted into pots. Transgenic plants were confirmed via PCR analysis using gene-specific primers.

Y2H assay

To screen the *H. brevisubulatum* complementary DNA library, the coding regions of *HbreCaBP* or *HbreFhb7* (Supplementary Data 16) were cloned into the pGBKT7 vector to create a bait construct, which was co-transformed with a prey cDNA library into the yeast strain AH109. The prey cDNA library was generated by fusing cDNAs from various *H. brevisubulatum* tissues into the pGADT7 vector. Transformants were selected using Quadruple DO medium (SD/-Leu/-Trp/-His/-Ade, -L-T-H-Ade).

Reporting summary

Further information on research design is available in the Nature Portfolio Reporting Summary linked to this article.

Data availability

Raw genome sequencing, population resequencing and RNA-seq data have been deposited in the National Center for Biotechnology Information Sequence Read Archive (SRA) database under the BioProject number PRJNA1005068. The I-genome assembly and annotation files are available in the Genome WareHouse database at the China National Genomics Data Center with BioProject accession number PRJCA019121. All additional data are provided in the main text or supplementary materials. Source data are provided with this paper.

Code availability

Custom codes used in this study have been deposited in GitHub at https://github.com/duqingwei1989/Hb_genome.

References

1. Lesk, C., Rowhani, P. & Ramankutty, N. Influence of extreme weather disasters on global crop production. *Nature* **529**, 84–87 (2016).
2. Lobell, D. B., Schlenker, W. & Costa-Roberts, J. Climate trends and global crop production since 1980. *Science* **333**, 616–620 (2011).
3. Myers, S. S. et al. Climate change and global food systems: potential impacts on food security and undernutrition. *Annu. Rev. Public Health* **38**, 259–277 (2017).
4. Gao, C. Genome engineering for crop improvement and future agriculture. *Cell* **184**, 1621–1635 (2021).
5. Zhang, F. & Batley, J. Exploring the application of wild species for crop improvement in a changing climate. *Curr. Opin. Plant Biol.* **56**, 218–222 (2020).
6. Bohra, A. et al. Reap the crop wild relatives for breeding future crops. *Trends Biotechnol.* **40**, 412–431 (2022).
7. Flourish with the wild. *Nat. Plants* **9**, 373–374 (2023).
8. Avila, C. M., Rodriguez-Suarez, C. & Atienza, S. G. *Tritordeum*: creating a new crop species—the successful use of plant genetic resources. *Plants* **10**, 1029 (2021).
9. Wang, Z. et al. Development and identification of an elite wheat-*Hordeum californicum* T6HcS/6BL translocation line ND646 containing several desirable traits. *Genet. Mol. Biol.* **45**, e20220117 (2022).
10. Brassac, J. & Blattner, F. R. Species-level phylogeny and polyploid relationships in *Hordeum* (Poaceae) inferred by next-generation sequencing and in silico cloning of multiple nuclear loci. *Syst. Biol.* **64**, 792–808 (2015).
11. Garthwaite, A. J., von Bothmer, R. & Colmer, T. D. Salt tolerance in wild *Hordeum* species is associated with restricted entry of Na^+ and Cl^- into the shoots. *J. Exp. Bot.* **56**, 2365–2378 (2005).
12. Zhang, H. W. et al. Emerging crosstalk between two signaling pathways coordinates K^+ and Na^+ homeostasis in the halophyte *Hordeum brevisubulatum*. *J. Exp. Bot.* **71**, 4345–4358 (2020).
13. Intergovernmental Technical Panel on Soils. *Status of the World's Soil Resources* (Food and Agriculture Organization of the United Nations, 2015); https://www.fao.org/3/i5199e/i5199e.pdf
14. Zhang, H. et al. A Gγ protein regulates alkaline sensitivity in crops. *Science* **379**, eade8416 (2023).
15. McCormack, E., Tsai, Y. C. & Braam, J. Handling calcium signaling: *Arabidopsis* CaMs and CMLs. *Trends Plant Sci.* **10**, 383–389 (2005).
16. Cao, Y. et al. Natural variation of an EF-hand Ca^{2+}-binding-protein coding gene confers saline–alkaline tolerance in maize. *Nat. Commun.* **11**, 186 (2020).
17. Chen, R. et al. Adaptive innovation of green plants by horizontal gene transfer. *Biotechnol. Adv.* **46**, 107671 (2021).
18. Wang, H. W. et al. Horizontal gene transfer of *Fhb7* from fungus underlies *Fusarium* head blight resistance in wheat. *Science* **368**, eaba5435 (2020).
19. Wang, X. et al. A recent burst of gene duplications in Triticeae. *Plant Commun.* **3**, 100268 (2022).
20. Middleton, C. P., Stein, N., Keller, B., Kilian, B. & Wicker, T. Comparative analysis of genome composition in Triticeae reveals strong variation in transposable element dynamics and nucleotide diversity. *Plant J.* **73**, 347–356 (2013).
21. Li, W., Zhang, P., Fellers, J. P., Friebe, B. & Gill, B. S. Sequence composition, organization, and evolution of the core Triticeae genome: composition and genome expansion in Triticeae. *Plant J.* **40**, 500–511 (2004).
22. Cheng, Y. et al. Chromosome-scale genome sequence of *Suaeda glauca* sheds light on salt stress tolerance in halophytes. *Hortic. Res.* **10**, uhad161 (2023).
23. van Ooijen, G. et al. Structure–function analysis of the NB-ARC domain of plant disease resistance proteins. *J. Exp. Bot.* **59**, 1383–1397 (2008).
24. Ahmed, H. I. et al. Einkorn genomics sheds light on history of the oldest domesticated wheat. *Nature* **620**, 830–838 (2023).
25. Kuraparthy, V., Sood, S., Dhaliwal, H. S., Chhuneja, P. & Gill, B. S. Identification and mapping of a tiller inhibition gene (*tin3*) in wheat. *Theor. Appl. Genet.* **114**, 285–294 (2007).
26. Tavakol, E. et al. The barley *Uniculme4* gene encodes a BLADE-ON-PETIOLE-like protein that controls tillering and leaf patterning. *Plant Physiol.* **168**, 164–174 (2015).
27. Jayakodi, M. et al. The barley pan-genome reveals the hidden legacy of mutation breeding. *Nature* **588**, 284–289 (2020).
28. Liu, M. et al. The draft genome of a wild barley genotype reveals its enrichment in genes related to biotic and abiotic stresses compared to cultivated barley. *Plant Biotechnol. J.* **18**, 443–456 (2020).
29. Zeng, X. Q. et al. Origin and evolution of qingke barley in Tibet. *Nat. Commun.* **9**, 5433 (2018).
30. Mascher, M. et al. Barley whole exome capture: a tool for genomic research in the genus *Hordeum* and beyond. *Plant J.* **76**, 494–505 (2013).
31. Fu, H. et al. SALT OVERLY SENSITIVE 1 is inhibited by clade D Protein phosphatase 2C D6 and D7 in *Arabidopsis thaliana*. *Plant Cell* **35**, 279–297 (2023).
32. Yang, Y. & Guo, Y. Unraveling salt stress signaling in plants. *J. Integr. Plant Biol.* **60**, 796–804 (2018).
33. Mascher, M. et al. Long-read sequence assembly: a technical evaluation in barley. *Plant Cell* **33**, 1888–1906 (2021).

34. Kamran, M., Ramesh, S. A., Gilliham, M., Tyerman, S. D. & Bose, J. Role of TaALMT1 malate-GABA transporter in alkaline pH tolerance of wheat. *Plant Cell Environ.* **43**, 2443–2459 (2020).
35. Li, M. et al. Plasma membrane-localized H^+-ATPase OsAHA3 functions in saline-alkaline stress tolerance in rice. *Plant Cell Rep.* **43**, 9 (2023).
36. Merot, C., Oomen, R. A., Tigano, A. & Wellenreuther, M. A roadmap for understanding the evolutionary significance of structural genomic variation. *Trends Ecol. Evol.* **35**, 561–572 (2020).
37. Ren, G. et al. The genome sequence provides insights into salt tolerance of *Achnatherum splendens* (Gramineae), a constructive species of alkaline grassland. *Plant Biotechnol. J.* **20**, 116–128 (2022).
38. Chen, S. et al. The *Spartina alterniflora* genome sequence provides insights into the salt-tolerance mechanisms of exo-recretohalophytes. *Plant Biotechnol. J.* **22**, 2558–2574 (2024).
39. Qin, P. et al. Pan-genome analysis of 33 genetically diverse rice accessions reveals hidden genomic variations. *Cell* **184**, 3542–3558 (2021).
40. Wu, S. J., Ding, L. & Zhu, J. K. SOS1, a genetic locus essential for salt tolerance and potassium acquisition. *Plant Cell* **8**, 617–627 (1996).
41. Oh, D. H. et al. Loss of halophytism by interference with *SOS1* expression. *Plant Physiol.* **151**, 210–222 (2009).
42. Kuang, L. et al. The genome and gene editing system of sea barleygrass provide a novel platform for cereal domestication and stress tolerance studies. *Plant Commun.* **3**, 100333 (2022).
43. Palmgren, M. G. Plant plasma membrane H^+-ATPases: powerhouses for nutrient uptake. *Annu. Rev. Plant Physiol. Plant Mol. Biol.* **52**, 817–845 (2001).
44. Gong, Z. et al. Plant abiotic stress response and nutrient use efficiency. *Sci. China. Life Sci.* **63**, 635–674 (2020).
45. Liu, J. et al. A natural variation in *SlSCaBP8* promoter contributes to the loss of saline-alkaline tolerance during tomato improvement. *Hortic. Res.* **11**, uhae055 (2024).
46. Zou, X., Liu, M. Y., Wu, W. H. & Wang, Y. Phosphorylation at Ser28 stabilizes the *Arabidopsis* nitrate transporter NRT2.1 in response to nitrate limitation. *J. Integr. Plant Biol.* **62**, 865–876 (2020).
47. Ohkubo, Y., Kuwata, K. & Matsubayashi, Y. A type 2C protein phosphatase activates high-affinity nitrate uptake by dephosphorylating NRT2.1. *Nat. Plants* **7**, 310–316 (2021).
48. Wang, T. et al. Brassinosteroid transcription factor BES1 modulates nitrate deficiency by promoting NRT2.1 and NRT2.2 transcription in *Arabidopsis*. *Plant J.* **114**, 1443–1457 (2023).
49. Luo, H. et al. Telomere-to-telomere genome of the allotetraploid legume *Sesbania cannabina* reveals transposon-driven subgenome divergence and mechanisms of alkaline stress tolerance. *Sci. China. Life Sci.* **67**, 149–160 (2024).
50. Guo, X., Wang, M., Kang, H., Zhou, Y. & Han, F. Distribution, polymorphism and function characteristics of the GST-encoding *Fhb7* in Triticeae. *Plants* **11**, 2074 (2022).
51. Tanaka, A., Takemoto, D., Chujo, T. & Scott, B. Fungal endophytes of grasses. *Curr. Opin. Plant Biol.* **15**, 462–468 (2012).
52. Shinozuka, H. et al. Horizontal transfer of a *β-1,6-glucanase* gene from an ancestral species of fungal endophyte to a cool-season grass host. *Sci. Rep.* **7**, 9024 (2017).
53. Yu, H. et al. A route to de novo domestication of wild allotetraploid rice. *Cell* **184**, 1156–1170 (2021).
54. Kokot, M., Dlugosz, M. & Deorowicz, S. KMC 3: counting and manipulating *k*-mer statistics. *Bioinformatics* **33**, 2759–2761 (2017).
55. Cheng, H., Concepcion, G. T., Feng, X., Zhang, H. & Li, H. Haplotype-resolved de novo assembly using phased assembly graphs with hifiasm. *Nat. Methods* **18**, 170–175 (2021).
56. Durand, N. C. et al. Juicer provides a one-click system for analyzing loop-resolution Hi-C experiments. *Cell Syst.* **3**, 95–98 (2016).
57. Dudchenko, O. et al. De novo assembly of the *Aedes aegypti* genome using Hi-C yields chromosome-length scaffolds. *Science* **356**, 92–95 (2017).
58. Stanke, M. et al. AUGUSTUS: ab initio prediction of alternative transcripts. *Nucleic Acids Res.* **34**, W435–W439 (2006).
59. Bolger, A. M., Lohse, M. & Usadel, B. Trimmomatic: a flexible trimmer for Illumina sequence data. *Bioinformatics* **30**, 2114–2120 (2014).
60. Kim, D., Paggi, J. M., Park, C., Bennett, C. & Salzberg, S. L. Graph-based genome alignment and genotyping with HISAT2 and HISAT-genotype. *Nat. Biotechnol.* **37**, 907–915 (2019).
61. International Wheat Genome Sequencing, Appels, R. et al. Shifting the limits in wheat research and breeding using a fully annotated reference genome. *Science* **361**, eaar7191 (2018).
62. Ou, S. et al. Benchmarking transposable element annotation methods for creation of a streamlined, comprehensive pipeline. *Genome Biol.* **20**, 275 (2019).
63. Tarailo-Graovac, M. & Chen, N. Using RepeatMasker to identify repetitive elements in genomic sequences. *Curr. Protoc. Bioinformatics* **4**, 4.10.1–4.10.14 (2009).
64. Ou, S. & Jiang, N. LTR_FINDER_parallel: parallelization of LTR_FINDER enabling rapid identification of long terminal repeat retrotransposons. *Mob. DNA* **10**, 48 (2019).
65. Ellinghaus, D., Kurtz, S. & Willhoeft, U. LTRharvest, an efficient and flexible software for *de novo* detection of LTR retrotransposons. *BMC Bioinformatics* **9**, 18 (2008).
66. Ou, S. & Jiang, N. LTR_retriever: a highly accurate and sensitive program for identification of long terminal repeat retrotransposons. *Plant Physiol.* **176**, 1410–1422 (2018).
67. Li, B. C. et al. Wheat centromeric retrotransposons: the new ones take a major role in centromeric structure. *Plant J.* **73**, 952–965 (2013).
68. Zhang, X. et al. A chromosome-scale genome assembly of *Dasypyrum villosum* provides insights into its application as a broad-spectrum disease resistance resource for wheat improvement. *Mol. Plant* **16**, 432–451 (2023).
69. Huang, N. & Li, H. compleasm: a faster and more accurate reimplementation of BUSCO. *Bioinformatics* **39**, btad595 (2023).
70. Li, L. F. et al. Genome sequences of five *Sitopsis* species of *Aegilops* and the origin of polyploid wheat B subgenome. *Mol. Plant* **15**, 488–503 (2022).
71. Ling, H. Q. et al. Genome sequence of the progenitor of wheat A subgenome *Triticum urartu*. *Nature* **557**, 424–428 (2018).
72. Zhou, Y. et al. Introgressing the *Aegilops tauschii* genome into wheat as a basis for cereal improvement. *Nat. Plants* **7**, 774–786 (2021).
73. Li, G. et al. A high-quality genome assembly highlights rye genomic characteristics and agronomically important genes. *Nat. Genet.* **53**, 574–584 (2021).
74. Kamal, N. et al. The mosaic oat genome gives insights into a uniquely healthy cereal crop. *Nature* **606**, 113–119 (2022).
75. Zhang, W. et al. A high-quality genome sequence of alkaligrass provides insights into halophyte stress tolerance. *Sci. China. Life Sci.* **63**, 1269–1282 (2020).
76. The International Brachypodium Initiative. Genome sequencing and analysis of the model grass *Brachypodium distachyon*. *Nature* **463**, 763–768 (2010).
77. International Rice Genome Sequencing Project., Sasaki, T. The map-based sequence of the rice genome. *Nature* **436**, 793–800 (2005).
78. Ming, R. et al. The pineapple genome and the evolution of CAM photosynthesis. *Nat. Genet.* **47**, 1435–1442 (2015).

79. Emms, D. M. & Kelly, S. OrthoFinder: phylogenetic orthology inference for comparative genomics. *Genome Biol.* **20**, 238 (2019).
80. Shen, F. et al. Comparative genomics reveals a unique nitrogen-carbon balance system in Asteraceae. *Nat. Commun.* **14**, 4334 (2023).
81. Zhang, X. T. et al. Genomes of the banyan tree and pollinator wasp provide insights into fig-wasp coevolution. *Cell* **183**, 875–889.e17 (2020).
82. Edgar, R. C. MUSCLE: multiple sequence alignment with high accuracy and high throughput. *Nucleic Acids Res.* **32**, 1792–1797 (2004).
83. Capella-Gutierrez, S., Silla-Martinez, J. M. & Gabaldon, T. trimAl: a tool for automated alignment trimming in large-scale phylogenetic analyses. *Bioinformatics* **25**, 1972–1973 (2009).
84. Minh, B. Q. et al. IQ-TREE 2: new models and efficient methods for phylogenetic inference in the genomic era. *Mol. Biol. Evol.* **37**, 1530–1534 (2020).
85. Mirarab, S. et al. ASTRAL: genome-scale coalescent-based species tree estimation. *Bioinformatics* **30**, i541–i548 (2014).
86. Darriba, D. et al. ModelTest-NG: a new and scalable tool for the selection of DNA and protein evolutionary models. *Mol. Biol. Evol.* **37**, 291–294 (2020).
87. Guindon, S. et al. New algorithms and methods to estimate maximum-likelihood phylogenies: assessing the performance of PhyML 3.0. *Syst. Biol.* **59**, 307–321 (2010).
88. De Bie, T., Cristianini, N., Demuth, J. P. & Hahn, M. W. CAFE: a computational tool for the study of gene family evolution. *Bioinformatics* **22**, 1269–1271 (2006).
89. Finn, R. D., Clements, J. & Eddy, S. R. HMMER web server: interactive sequence similarity searching. *Nucleic Acids Res.* **39**, W29–W37 (2011).
90. Kozlov, A. M., Darriba, D., Flouri, T., Morel, B. & Stamatakis, A. RAxML-NG: a fast, scalable and user-friendly tool for maximum likelihood phylogenetic inference. *Bioinformatics* **35**, 4453–4455 (2019).
91. Lovell, J. T. et al. GENESPACE tracks regions of interest and gene copy number variation across multiple genomes. *eLife* **11**, e78526 (2022).
92. Buchfink, B., Reuter, K. & Drost, H.-G. Sensitive protein alignments at tree-of-life scale using DIAMOND. *Nat. Methods* **18**, 366–368 (2021).
93. Zwaenepoel, A. & Van de Peer, Y. Inference of ancient whole-genome duplications and the evolution of gene duplication and loss rates. *Mol. Biol. Evol.* **36**, 1384–1404 (2019).
94. Qiao, X. et al. Gene duplication and evolution in recurring polyploidization-diploidization cycles in plants. *Genome Biol.* **20**, 38 (2019).
95. Andrews, S. FastQC a quality control tool for high throughput sequence data (Babraham Institute, 2014); https://www.bioinformatics.babraham.ac.uk/projects/fastqc/
96. Danecek, P. et al. The variant call format and VCFtools. *Bioinformatics* **27**, 2156–2158 (2011).
97. Narasimhan, V. et al. BCFtools/RoH: a hidden Markov model approach for detecting autozygosity from next-generation sequencing data. *Bioinformatics* **32**, 1749–1751 (2016).
98. Yang, J., Lee, S. H., Goddard, M. E. & Visscher, P. M. GCTA: a tool for genome-wide complex trait analysis. *Am. J. Hum. Genet.* **88**, 76–82 (2011).
99. Alexander, D. H., Novembre, J. & Lange, K. Fast model-based estimation of ancestry in unrelated individuals. *Genome Res.* **19**, 1655–1664 (2009).
100. Pavlidis, P., Zivkovic, D., Stamatakis, A. & Alachiotis, N. SweeD: likelihood-based detection of selective sweeps in thousands of genomes. *Mol. Biol. Evol.* **30**, 2224–2234 (2013).
101. Pickrell, J. K. & Pritchard, J. K. Inference of population splits and mixtures from genome-wide allele frequency data. *PLoS Genet.* **8**, e1002967 (2012).
102. Fitak, R. R. OptM: estimating the optimal number of migration edges on population trees using Treemix. *Biol. Methods Protoc.* **6**, bpab017 (2021).
103. Malinsky, M., Matschiner, M. & Svardal, H. Dsuite - fast *D*-statistics and related admixture evidence from VCF files. *Mol. Ecol. Resour.* **21**, 584–595 (2021).
104. Pedersen, B. S. & Quinlan, A. R. Mosdepth: quick coverage calculation for genomes and exomes. *Bioinformatics* **34**, 867–868 (2018).
105. Maccaferri, M. et al. Durum wheat genome highlights past domestication signatures and future improvement targets. *Nat. Genet.* **51**, 885–895 (2019).
106. Dobin, A. et al. STAR: ultrafast universal RNA-seq aligner. *Bioinformatics* **29**, 15–21 (2013).
107. Liao, Y., Smyth, G. K. & Shi, W. featureCounts: an efficient general purpose program for assigning sequence reads to genomic features. *Bioinformatics* **30**, 923–930 (2014).
108. Langfelder, P. & Horvath, S. WGCNA: an R package for weighted correlation network analysis. *BMC Bioinformatics* **9**, 559 (2008).
109. Ramirez-Gonzalez, R. H. et al. The transcriptional landscape of polyploid wheat. *Science* **361**, eaar6089 (2018).
110. Liu, Y., Hu, B. & Chu, C. ^{15}N-nitrate uptake activity and root-to-shoot transport assay in rice. *Bio Protoc.* **6**, e1897 (2016).
111. Chen, K. E., Chen, H. Y., Tseng, C. S. & Tsay, Y. F. Improving nitrogen use efficiency by manipulating nitrate remobilization in plants. *Nat. Plants* **6**, 1126–1135 (2020).
112. Bartlett, J. G., Alves, S. C., Smedley, M., Snape, J. W. & Harwood, W. A. High-throughput *Agrobacterium*-mediated barley transformation. *Plant Methods* **4**, 22 (2008).

Acknowledgements

We thank the National Wheat Wild Relative Resource Garden of China, the National Herbage Germplasm Bank of China and the US National Plant Germplasm Bank for kindly providing the *Hordeum* I-genome accessions. We thank P. Yang and Q. Shen for providing barley cv. Golden Promise seeds. We thank H. Du, H. Lu, H. Liu and G. Liu for their technical support in genome assembly and annotation. We thank X. Wang and F. Lu for their helpful suggestions and comments on the manuscript. This work was supported by grants from the Natural Science Foundation of Beijing (5222006 to R.L.), the Outstanding Scientist Development Program of Beijing Academy of Agriculture and Forestry Sciences (JKZX202203 to R.L.), the Collaboration and Science and Technology Innovation Project of Beijing Academy of Agriculture and Forestry Sciences (KJCX201907-2 to R.L.), the Innovation Program of Beijing Academy of Agriculture and Forestry Sciences (KJCX20230117 to Y. Jiang, KJCX20230404 to H.F.) and the National Natural Science Foundation of China (32101710 to H.F., 31771769 to R.L., 31801433 to Y. Jiang).

Author contributions

R.L. conceived this project and coordinated research activities. R.L., H.F., J.W., C.L. and Xingtan Zhang designed the experiments. R.L. and H.F. collected accessions and germplasms. H.F. and Y. Jiang isolated DNA and RNA and performed genome sequencing. Xingtan Zhang, Y.W., J.Y. and M.J. assembled and annotated the genomes. Q.D. and H.F. performed RNA-seq analysis and analysed gene families. Q.D., H.F., Y. Jia, B.C., Y.W. and V.G. performed population genetics analyses for genomic evolution, features, population structure and genetic diversity. Q.D., H.F., Y. Jia and B.C. performed comparative genomic analysis and population-based gene copy number variant analysis. H.F., Y. Jiang, H.Z., M.G.,

S.G., Xinjie Zhang and Y.S. generated barley transgenic lines and performed phenotypic analyses. H.F. and Q.D. prepared the figures and tables. H.F., Q.D. and R.L. wrote the manuscript. T.H., Y. Jia, R.K.V. and C.L. revised the manuscript. J.W., C.L., Xingtan Zhang and R.L. supervised the study.

Competing interests
The authors declare no competing interests.

Additional information
Extended data is available for this paper at https://doi.org/10.1038/s41477-025-01942-w.

Supplementary information The online version contains supplementary material available at https://doi.org/10.1038/s41477-025-01942-w.

Correspondence and requests for materials should be addressed to Jianhua Wei, Chengdao Li, Xingtan Zhang or Ruifen Li.

Peer review information *Nature Plants* thanks Frank Blattner and the other, anonymous, reviewer(s) for their contribution to the peer review of this work.

Reprints and permissions information is available at www.nature.com/reprints.

Publisher's note Springer Nature remains neutral with regard to jurisdictional claims in published maps and institutional affiliations.

Open Access This article is licensed under a Creative Commons Attribution-NonCommercial-NoDerivatives 4.0 International License, which permits any non-commercial use, sharing, distribution and reproduction in any medium or format, as long as you give appropriate credit to the original author(s) and the source, provide a link to the Creative Commons licence, and indicate if you modified the licensed material. You do not have permission under this licence to share adapted material derived from this article or parts of it. The images or other third party material in this article are included in the article's Creative Commons licence, unless indicated otherwise in a credit line to the material. If material is not included in the article's Creative Commons licence and your intended use is not permitted by statutory regulation or exceeds the permitted use, you will need to obtain permission directly from the copyright holder. To view a copy of this licence, visit http://creativecommons.org/licenses/by-nc-nd/4.0/.

© The Author(s) 2025

https://doi.org/10.1038/s41477-025-01942-w

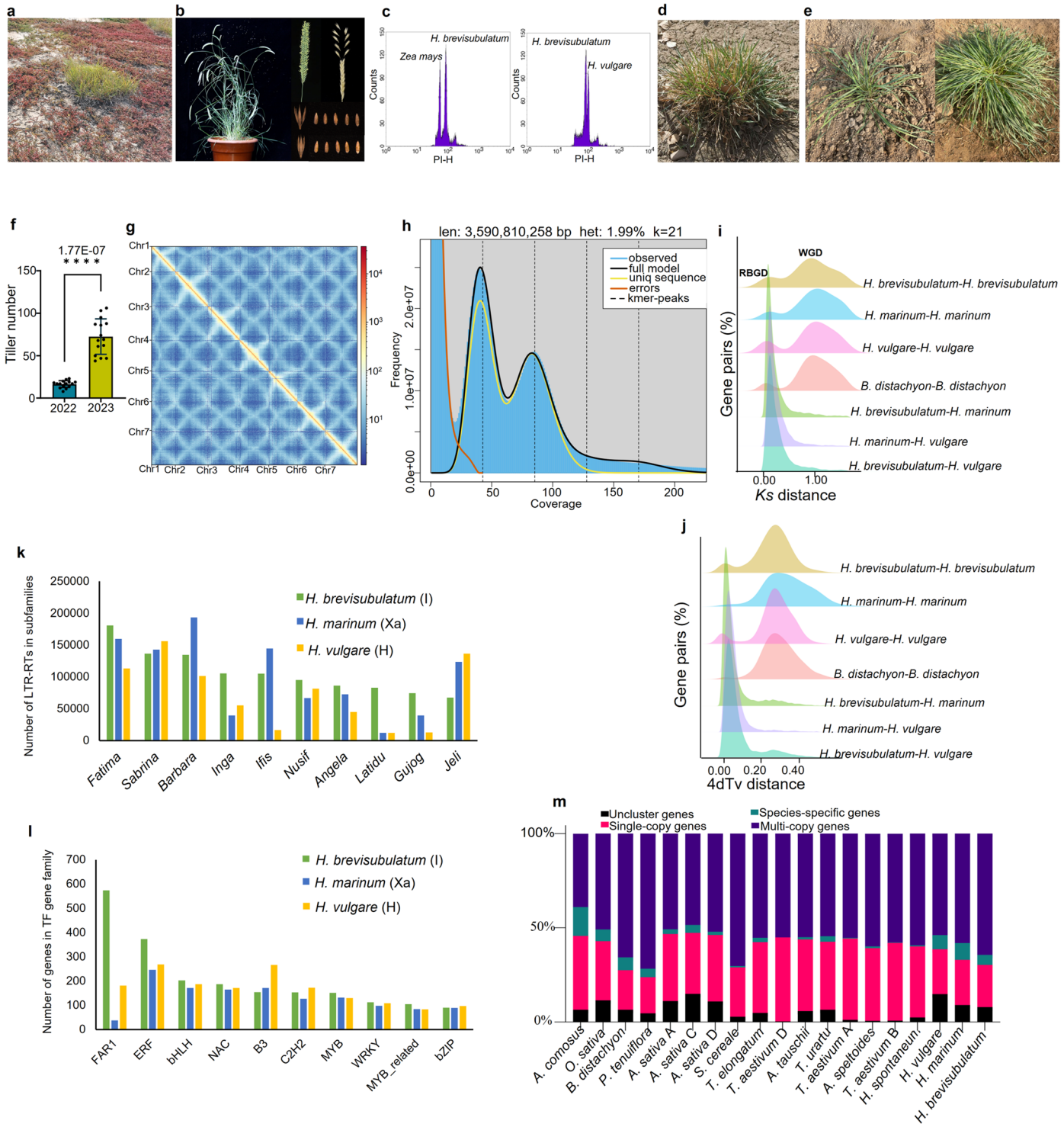

Extended Data Fig. 1 | See next page for caption.

https://doi.org/10.1038/s41477-025-01942-w

Extended Data Fig. 1 | Genomic features of *H. brevisubulatum* genome. **a**, *H. brevisubulatum* plants (green), which have been growing for multiple years, in heavily alkaline salinity-affected soil around mid-September. Red plants represent *Suaeda salsa*, an indicator of heavily alkali-affected soil. **b**, The pot cultivation of *H. brevisubulatum* (left), the phenotype of spikes and seeds (right). **c**, A histogram of relative fluorescence intensities from flow cytometric analysis of propidium iodide (PI)-stained nuclei was generated for *H. brevisubulatum* accession PI 531775. *Zea mays* cv B73 (2n = 2x = ~2.3 Gb) and *H. vulgare* cv Morex (2n = 2x = ~5.04 Gb) served as internal reference standards. The average peak fluorescence ratios of *H. brevisubulatum* to *Z. mays* and *H. vulgare* were 1.587 and 0.748, respectively, resulting in an estimated genome size for *H. brevisubulatum* of ~3.65–3.77 Gb. **d**, Regrowth of *H. brevisubulatum* in early Spring in Beijing. **e**, Growth status of the same *H. brevisubulatum* plant in two consecutive years: 2022 (left) and 2023 (right). Increased tillering was observed in 2023. **f**, Quantification of tiller numbers in Extended Data Fig. 1d. The error bars represent mean ± S.D. with n = 15 biological replicates. Significant differences were determined using a two-tailed Student's *t*-test (****P < 0.0001). **g**, Genome-wide interaction heat map of Hi-C links among seven chromosomes. **h**, Estimation of genome size and heterozygosity based on 21-mer frequency distribution analysis. **i**, The distribution of *Ks* values of intragenomic and intergenomic collinearity gene pairs among *H. brevisubulatum*, *H. marinum*, *H. vulgare*, and *Brachypodium distachyon*. **j**, The distribution of the transversion rates at the 4dTv of intragenomic and intergenomic collinearity gene pairs among *H. brevisubulatum*, *H. marinum*, *H. vulgare*, and *B. distachyon*. **k**, Number of LTR-RTs in the top 10 LTR subfamilies that were identified in the I genome (*H. brevisubulatum*), Xa genome (*H. marinum*), and H genome (*H. vulgare*). **l**, The top 10 transcriptional factor gene families were identified in the I genome (*H. brevisubulatum*), Xa genome (*H. marinum*), and H genome (*H. vulgare*). **m**, Summary of unclustered, species-specific, multi-copy and single-copy genes in 19 genomes based on OrthoFinder analysis. Source data are provided as a source data file.

https://doi.org/10.1038/s41477-025-01942-w

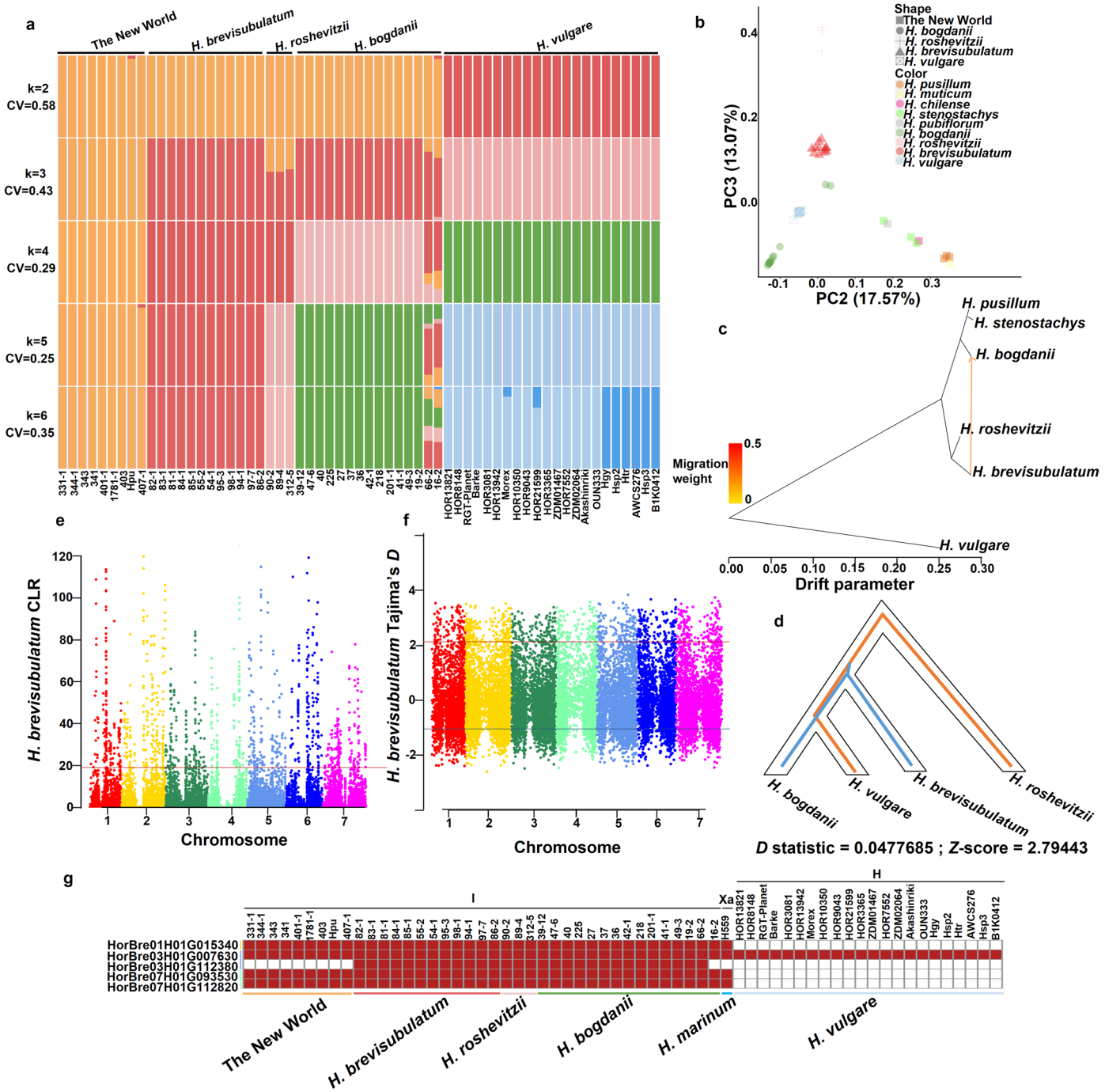

Extended Data Fig. 2 | Population structure and genomic diversity of the I genome. a, Population structures were estimated using Admixture software with ancestral population sizes k = 2-6, and the k = 5 with the lowest cross-validation error (CV = 0.25) was selected as the optimal population clustering group. **b**, PCA analysis of 61 accessions illustrating the results of PC2 versus PC3 (including 12 *H. brevisubulatum*, 15 *H. bogdanii*, three *H. roshevitzii*, nine accessions from the New World and 22 barley accessions). The classifications of species are represented by shapes or colors. **c**, TreeMix analysis of the gene flow among the I-genome groups and H-genome groups. **d**, The four-taxon ABBA/BABA test of introgression was conducted with the excess of shared derived alleles (represented by *D* values and *Z*-scores) listed on the bottom. **e, f**, Genome-wide distribution of CLR (e) and Tajima's *D* (f) of *H. brevisubulatum* accessions along 7 chromosomes, red line represents the threshold of the top 5% CLR and the top 2.5% Tajima's *D*, blue line represents the threshold of the bottom 2.5% Tajima's *D*. **g**, Distribution of the five copies of *SOS1* among *Hordeum* I, Xa and H species. Source data are provided as a source data file.

https://doi.org/10.1038/s41477-025-01942-w

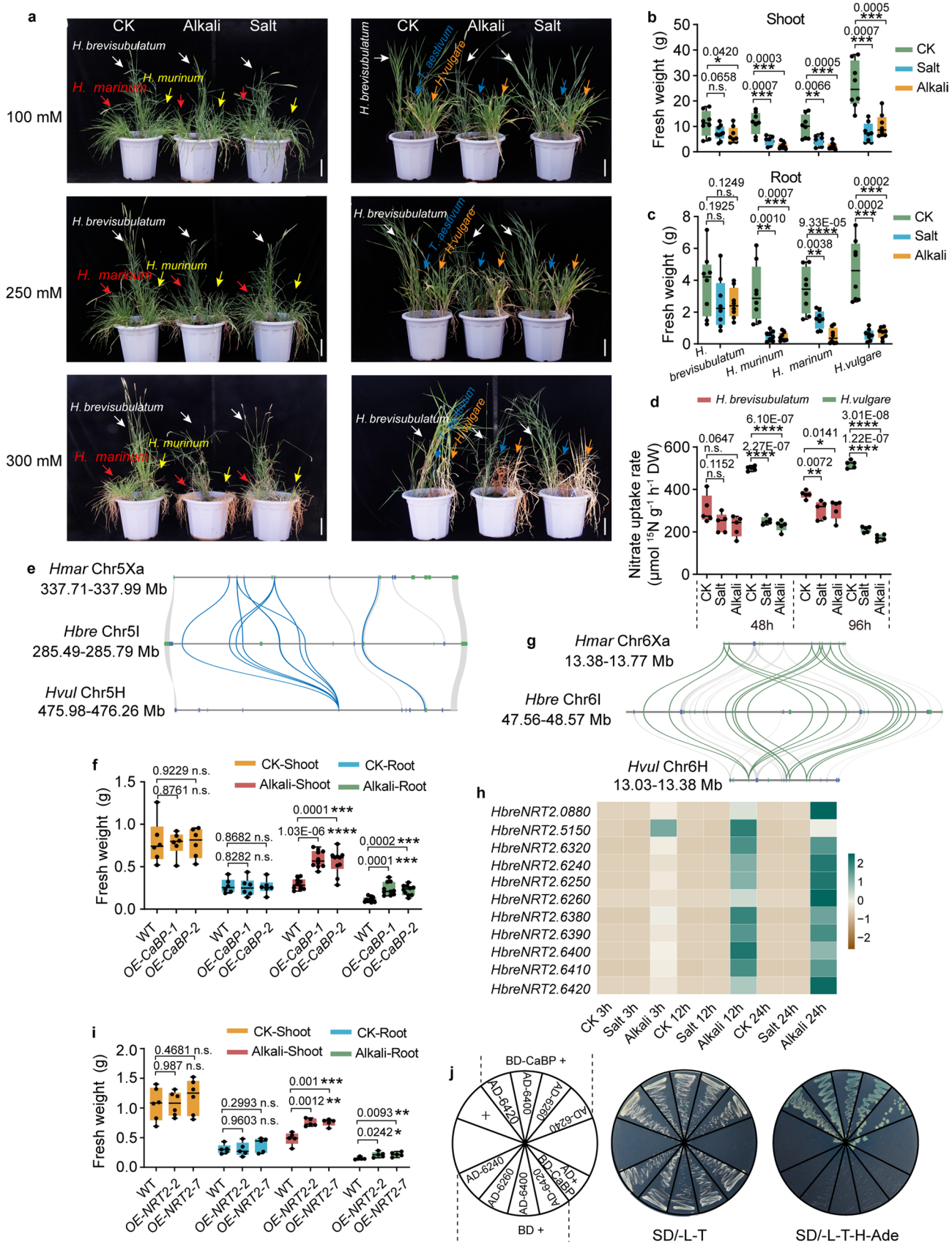

Extended Data Fig. 3 | See next page for caption.

https://doi.org/10.1038/s41477-025-01942-w

Extended Data Fig. 3 | Phenotype of superior tolerance to alkali stress and duplicate CaBP-NRT2 module identified in *H. brevisubulatum*. **a**, Comparison of phenotypic changes of different *Hordeum* species under salt and alkali stresses for 21 days. *H. brevisubulatum* (PI531775, white arrow); *H. marinum* (PI 200341, red arrow); *H. murinum* (PI 266198, yellow arrow); *H. vulgare* cv. Golden Promise (orange arrow); *T. aestivum* cv. Zhoumai30 (blue arrow). Bar = 10 cm. **b, c**, Shoot (b) and root (c) fresh weight of the four *Hordeum* species under salt and alkali stresses for 21 days. **d**, Comparison of nitrate uptake rate between *H. brevisubulatum* and *H. valgare* under salt and alkali stresses for 48 or 96 hrs. **e**, Comparison of microsynteny in *CaBP* loci among *Hordeum* genome. **f**, Fresh weight of *CaBP* transgenic plants under alkali stress. **g**, Comparison of microsynteny in *NRT2* loci among *Hordeum* genome. **h**, Heat map showing the expression patterns of *HbreNRT2s* in response to salt and alkali stresses in the roots of *H. brevisubulatum*. **i**, Fresh weight of *HbreNRT2* transgenic plants under alkali stress. **j**, The interaction of CaBP with NRT2 was identified by yeast two-hybrid assay (Y2H). The left panel shows the sample name layout. AD and BD refer to the empty vector control. '+' symbol indicates the positive control. BD-CaBP refers to *HbreCaBP* fused downstream to the BD domain of pGBKT7 as bait. AD-6420, et. al. (AD-IDs) refer to the *HbreNRT2* gene IDs. The truncated *HbreNRT2s* were fused downstream to the AD domain of pGADT7 as preys. The Y2H experiments were performed by co-transformation of bait and preys and grown on selective medium. The growth on SD/-L-T indicates that the bait and prey were transformed into the yeast strain (mid panel), and the growth on SD/-L-T-H-Ade indicates interaction between the bait and prey (right panel). SD/-L-T stands for selective medium lacking Leu and Trp. SD/-L-T-H-Ade stands for the selective medium lacking Leu, Trp, His, and Ade. Boxplots show the median, 25th–75th interquartile range (IQR), and minima and maxima (whiskers). Biological replicate numbers (n) are as follows: n = 8 for (b) and (c); n = 5 for (d); n = 6 for CK-Shoot and CK-Root, and n = 10 for Alkali-Shoot and Alkali-Root in (f); n = 6 for CK-Shoot, CK-Root and Alkali-Root, and n = 5 for Alkali-Shoot in (i). Significant differences were calculated using a two-tailed Student's *t*-test (*$P < 0.05$, **$P < 0.01$, ***$P < 0.001$, ****$P < 0.0001$, NS, non-significant). Source data are provided as a source data file.

https://doi.org/10.1038/s41477-025-01942-w

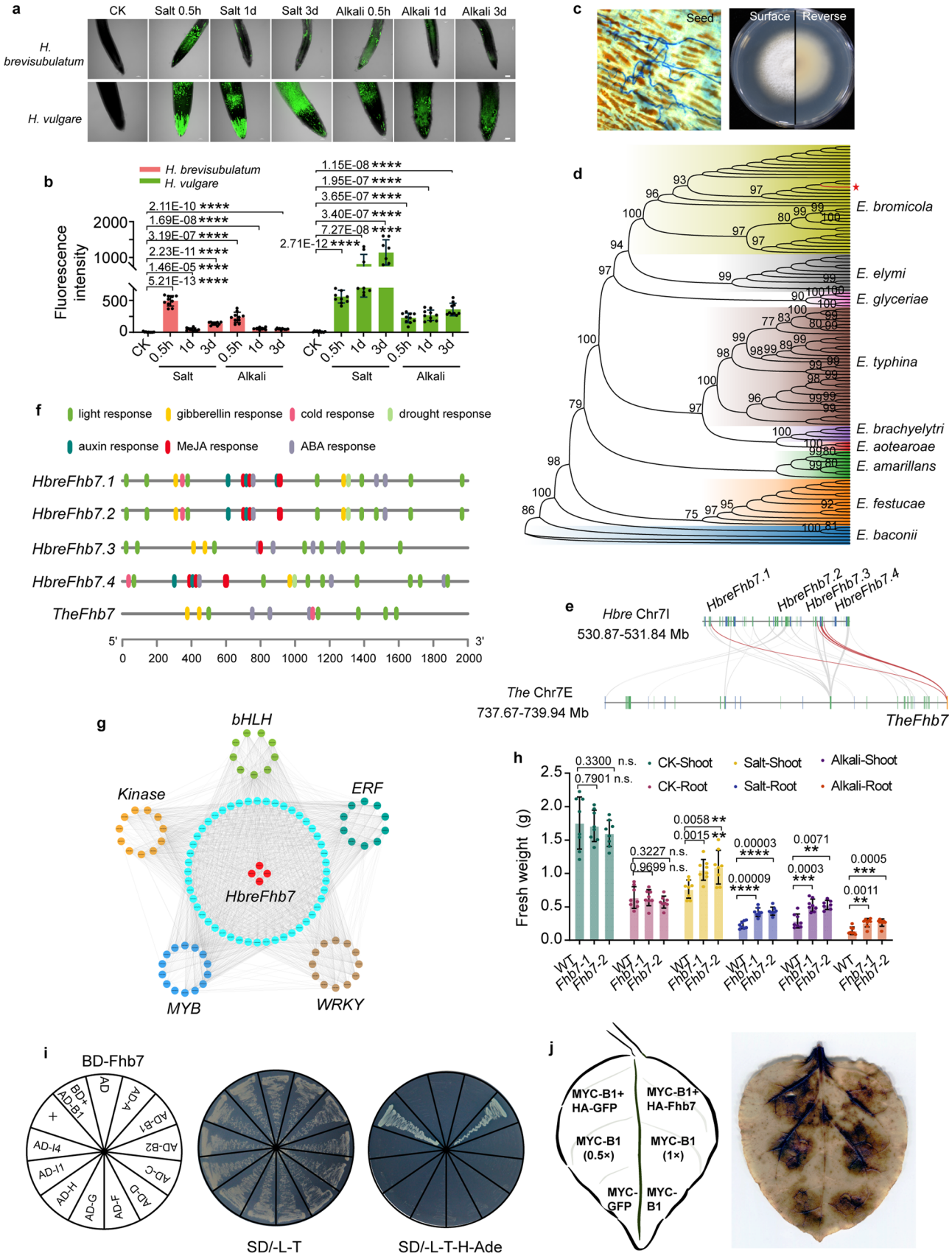

Extended Data Fig. 4 | See next page for caption.

https://doi.org/10.1038/s41477-025-01942-w

Extended Data Fig. 4 | *HbreFhb7* horizontally transferred from endophytic fungus innovates saline-alkaline tolerance by suppressing ROS accumulation. **a**, Comparison of ROS accumulation in roots of *H. brevisubulatum* and *H. vulgare* under alkali and salt stresses at each time point (0.5 h, 1 day, and 3 days). Bar = 100 μm. **b**, Quantification of the relative fluorescence intensity of the roots stained with H2DCFDA. **c**, *Epichloë* strains observed and isolated from the seeds of *H. bogdanii* in the Old World. **d**, Phylogenetic relationship of *Epichloë* strain in (d) with other plant endophytic fungi. Red asterisks indicating the strain isolated from the seeds of the I-genome species from the Old World. **e**, Comparison of microsynteny between *Fhb7* loci in *H. brevisubulatum* and *Thinopyrum elongatum*. **f**, Distribution of *cis*-elements within each *Fhb7* promoter. The 2000-bp DNA fragments upstream of ATG were analyzed using online software PlantCARE. **g**, Weighted Gene Co-expression Network Analysis (WGCNA) revealing that transcription factors represented by *WRKY*, *bHLH*, *ERF*, and *MYB*, as well as kinases-encoding genes, may co-express with *HbreFhb7*. **h**, Fresh weight of *HbreFhb7* transgenic plants under salt and alkali stresses. **i**, Interaction between HbreFhb7 and HbreRBOHs was identified by yeast two-hybrid assay (Y2H). The left panel shows the sample name layout. AD and BD refer to the empty vector control. '+' symbol indicates the positive control. BD-Fhb7 refers to *HbreFhb7* fused downstream to the BD domain of pGBKT7 as bait. AD-B1, et. al. (AD-IDs) refer to the *HbreRBOH* gene IDs. The truncated *HbreRBOH* were fused downstream to the AD domain of pGADT7 as preys. The Y2H experiments were performed by co-transformation of bait and preys and grown on selective medium. The growth on SD/-L-T indicates that the bait and prey were transformed into the yeast strain (mid panel), and the growth on SD/-L-T-H-Ade indicates interaction between the bait and prey (right panel). SD/-L-T stands for selective medium lacking Leu and Trp. SD/-L-T-H-Ade stands for the selective medium lacking Leu, Trp, His, and Ade. **j**, Co-expression of *HbreFhb7* with *HbreRBOHB1* leading to suppress ROS accumulation in tobacco leaves visualized by DAB staining. Expressing MYC-B1 accumulated more ROS than control MYC-GFP (bottom), and elevated expression of MYC-B1 (1× compared to 0.5×) accumulated more ROS (middle); while co-expression of *HbreFhb7* with *HbreRBOHB1* suppress ROS accumulation (top). The error bars represent mean ± S.D. with n = 12 biological replicates for (b), and n = 8 for (h). Significant differences were calculated using a two-tailed Student's *t*-test (***P* < 0.01, ****P* < 0.001, *****P* < 0.0001, NS, non-significant). Source data are provided as a source data file.

https://doi.org/10.1038/s41477-025-01942-w

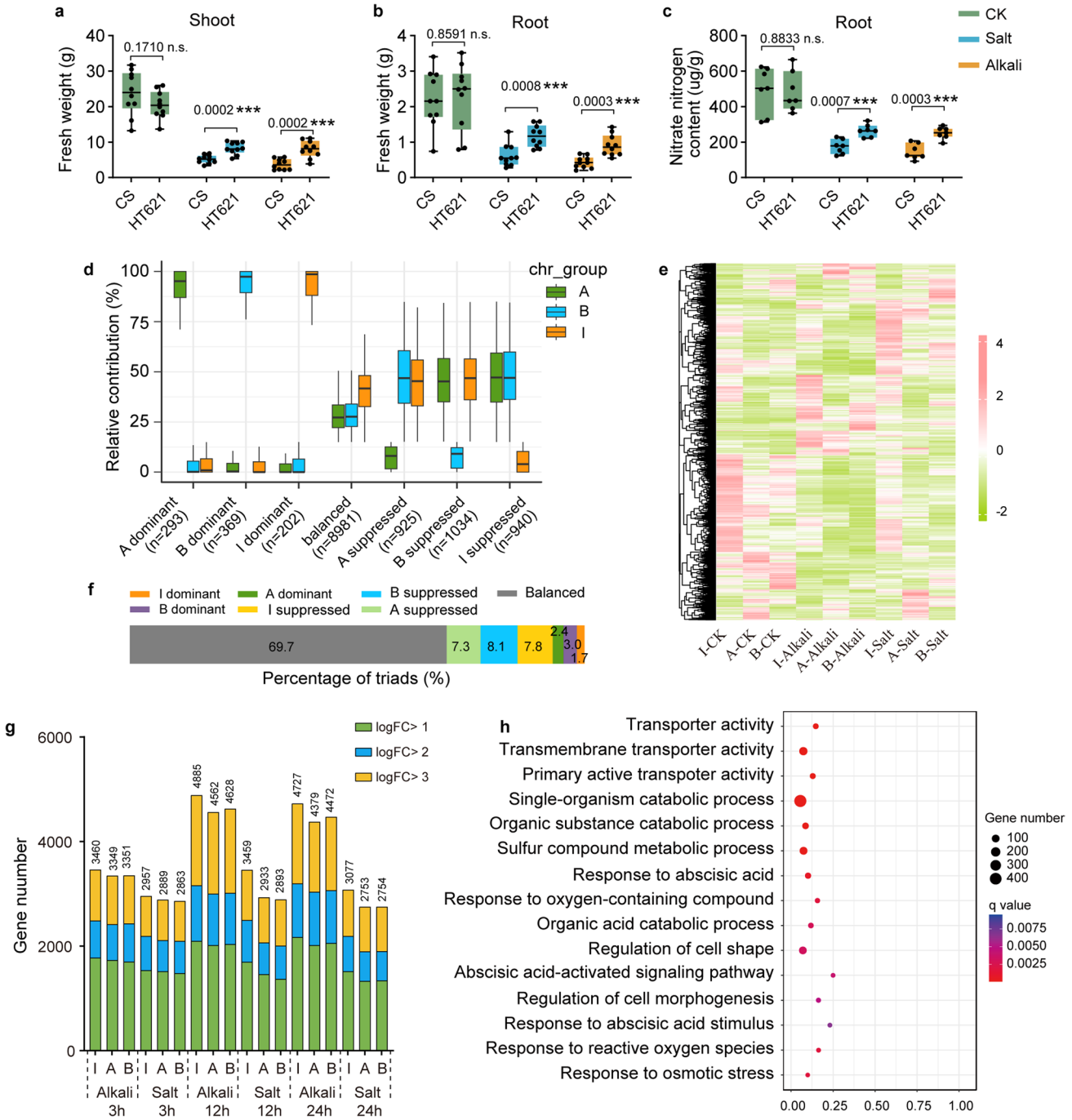

Extended Data Fig. 5 | Phenotypic difference and gene expression pattern of *Tritordeum* HT621 under alkali and salt stresses. a, b, Shoot (a) and root (b) fresh weight of HT621 and CS under alkali and salt stresses. **c**, Nitrate nitrogen content in roots of HT621 and CS under alkali and salt stresses. **d**, Box plots representing the relative contribution of each subgenome based on triad assignment to the seven categories. Gene number in each triad (n) was provided. **e**, Heat map showing the expression patterns of ancestral triads in the A, B, and I subgenomes of HT621 in response to alkali and salt stresses in roots. **f**, Gene expression patterns in ancestral triads of the A, B, and I subgenomes of HT621. **g**, Bar graph showing the number of markedly differentially expressed genes in the A, B and I subgenomes of HT621 during three time points of alkali and salt stresses in roots. **h**, Representative GO enrichment of the specifically up-regulated genes in the I subgenome of HT621 under alkali and salt stresses. Boxplots show the median, 25th–75th IQR, and minima and maxima (whiskers) with n = 10 biological replicates for (a) and (b), and n = 7 biological replicates for (c). Significant differences were calculated using a two-tailed Student's *t*-test (***$P < 0.001$, NS, non-significant). Source data are provided as a source data file.

nature portfolio

Corresponding author(s): Ruifen Li

Last updated by author(s): Jan 24, 2025

Reporting Summary

Nature Portfolio wishes to improve the reproducibility of the work that we publish. This form provides structure for consistency and transparency in reporting. For further information on Nature Portfolio policies, see our Editorial Policies and the Editorial Policy Checklist.

Statistics

For all statistical analyses, confirm that the following items are present in the figure legend, table legend, main text, or Methods section.

n/a	Confirmed
☐	☒ The exact sample size (*n*) for each experimental group/condition, given as a discrete number and unit of measurement
☐	☒ A statement on whether measurements were taken from distinct samples or whether the same sample was measured repeatedly
☐	☒ The statistical test(s) used AND whether they are one- or two-sided *Only common tests should be described solely by name; describe more complex techniques in the Methods section.*
☐	☒ A description of all covariates tested
☐	☒ A description of any assumptions or corrections, such as tests of normality and adjustment for multiple comparisons
☐	☒ A full description of the statistical parameters including central tendency (e.g. means) or other basic estimates (e.g. regression coefficient) AND variation (e.g. standard deviation) or associated estimates of uncertainty (e.g. confidence intervals)
☐	☒ For null hypothesis testing, the test statistic (e.g. *F*, *t*, *r*) with confidence intervals, effect sizes, degrees of freedom and *P* value noted *Give P values as exact values whenever suitable.*
☐	☒ For Bayesian analysis, information on the choice of priors and Markov chain Monte Carlo settings
☐	☒ For hierarchical and complex designs, identification of the appropriate level for tests and full reporting of outcomes
☒	☐ Estimates of effect sizes (e.g. Cohen's *d*, Pearson's *r*), indicating how they were calculated

Our web collection on statistics for biologists contains articles on many of the points above.

Software and code

Policy information about availability of computer code

Data collection	NO software was used for the data collection.
Data analysis	Juicer v1.8.9 3D-DNA v180419 Augustus v2.5.5 Trimmomatic v0.40 HiSAT2 v2.2.1 genewise v2.4.1 EDTA v2.0.0 RepeatModeler v2.0.4 RepeatMasker v4.1.5 OrthoFinder v2.5.4,PhyML v3.0 CAFE v4.2.1 Hmmer v3.3.2 RAxML-NG genespace Diamond v2.1.8 wgd v1.1.2 DupGen_finder FastQC v0.12.1 bwa v0.7.17

SAMtools v 1.17
GATK v 4.4.0.0
VCFtools v0.1.16
ModelTest-NG v 0.1.6
GCTA v1.94.1
Admixture v1.3.0
PopLDdecay
SweeD v3.3.1
TreeMix v 1.13
Dsuite v 0.5
Mosdepth v0.3.3
STAR v2.7.10
featureCounts v2.0.4

For manuscripts utilizing custom algorithms or software that are central to the research but not yet described in published literature, software must be made available to editors and reviewers. We strongly encourage code deposition in a community repository (e.g. GitHub). See the Nature Portfolio guidelines for submitting code & software for further information.

Data

Policy information about availability of data

All manuscripts must include a data availability statement. This statement should provide the following information, where applicable:

- Accession codes, unique identifiers, or web links for publicly available datasets
- A description of any restrictions on data availability
- For clinical datasets or third party data, please ensure that the statement adheres to our policy

Raw genome sequencing, population resequencing, and RNA-seq data have been deposited in the National Center for Biotechnology Information (NCBI) SRA database under the BioProject number PRJNA1005068. The I-genome assembly and annotation files are available in the Genome WareHouse database at the China National Genomics Data Center with BioProject accession number PRJCA019121. All additional data are provided in the main text or supplemental materials. Source data are provided with this paper.

Research involving human participants, their data, or biological material

Policy information about studies with human participants or human data. See also policy information about sex, gender (identity/presentation), and sexual orientation and race, ethnicity and racism.

Reporting on sex and gender	N/A
Reporting on race, ethnicity, or other socially relevant groupings	N/A
Population characteristics	N/A
Recruitment	N/A
Ethics oversight	N/A

Note that full information on the approval of the study protocol must also be provided in the manuscript.

Field-specific reporting

Please select the one below that is the best fit for your research. If you are not sure, read the appropriate sections before making your selection.

☒ Life sciences ☐ Behavioural & social sciences ☐ Ecological, evolutionary & environmental sciences

For a reference copy of the document with all sections, see nature.com/documents/nr-reporting-summary-flat.pdf

Life sciences study design

All studies must disclose on these points even when the disclosure is negative.

Sample size	The genome of a superior alkaline-saline tolerant H. brevisubulatum line (accession PI 531775, 2n = 2× = 14) was sequenced. 38 representative diploid Hordeum I genome accessions were re-sequenced.
Data exclusions	All sequencing data generated as raw data was used in the genome assembly and analyses.
Replication	Replications were used in the plant transformation, RNA-seq and functional characterization. The number of biological replicates is indicated in the figure legends.

Randomization	No randomization were involved in our study.
Blinding	No experiment involved in the blinding were carried out.

Reporting for specific materials, systems and methods

We require information from authors about some types of materials, experimental systems and methods used in many studies. Here, indicate whether each material, system or method listed is relevant to your study. If you are not sure if a list item applies to your research, read the appropriate section before selecting a response.

Materials & experimental systems

n/a	Involved in the study
☒	☐ Antibodies
☒	☐ Eukaryotic cell lines
☒	☐ Palaeontology and archaeology
☒	☐ Animals and other organisms
☒	☐ Clinical data
☒	☐ Dual use research of concern
☐	☒ Plants

Methods

n/a	Involved in the study
☒	☐ ChIP-seq
☐	☒ Flow cytometry
☒	☐ MRI-based neuroimaging

Dual use research of concern

Policy information about dual use research of concern

Hazards

Could the accidental, deliberate or reckless misuse of agents or technologies generated in the work, or the application of information presented in the manuscript, pose a threat to:

No	Yes	
☒	☐	Public health
☒	☐	National security
☒	☐	Crops and/or livestock
☒	☐	Ecosystems
☒	☐	Any other significant area

Experiments of concern

Does the work involve any of these experiments of concern:

No	Yes	
☒	☐	Demonstrate how to render a vaccine ineffective
☒	☐	Confer resistance to therapeutically useful antibiotics or antiviral agents
☒	☐	Enhance the virulence of a pathogen or render a nonpathogen virulent
☒	☐	Increase transmissibility of a pathogen
☒	☐	Alter the host range of a pathogen
☒	☐	Enable evasion of diagnostic/detection modalities
☒	☐	Enable the weaponization of a biological agent or toxin
☒	☐	Any other potentially harmful combination of experiments and agents

Plants

Seed stocks

Report on the source of all seed stocks or other plant material used. If applicable, state the seed stock centre and catalogue number. If plant specimens were collected from the field, describe the collection location, date and sampling procedures.

Novel plant genotypes

Describe the methods by which all novel plant genotypes were produced. This includes those generated by transgenic approaches, gene editing, chemical/radiation-based mutagenesis and hybridization. For transgenic lines, describe the transformation method, the number of independent lines analyzed and the generation upon which experiments were performed. For gene-edited lines, describe the editor used, the endogenous sequence targeted for editing, the targeting guide RNA sequence (if applicable) and how the editor was applied.

Authentication

Describe any authentication procedures for each seed stock used or novel genotype generated. Describe any experiments used to assess the effect of a mutation and, where applicable, how potential secondary effects (e.g. second site T-DNA insertions, mosiacism, off-target gene editing) were examined.

Flow Cytometry

Plots

Confirm that:

☒ The axis labels state the marker and fluorochrome used (e.g. CD4-FITC).

☒ The axis scales are clearly visible. Include numbers along axes only for bottom left plot of group (a 'group' is an analysis of identical markers).

☐ All plots are contour plots with outliers or pseudocolor plots.

☐ A numerical value for number of cells or percentage (with statistics) is provided.

Methodology

Sample preparation

Place ~20 mg of plant tissue into a plastic Petri dish. Add 1 ml of ice-cold nuclei isolation buffer. Immediately chop the tissue with a sharp razor blade or scalpel. Pipette the mixture up and down to homogenize (avoid air bubbles). Filter through a 42-µm nylon mesh into a labeled sample tube. Add PI (50 µg/ml) and RNase (50 µg/ml), then shake gently. Incubate the sample on ice for 5 minutes to 1 hour, shaking occasionally.

Instrument

BD FacsCalibur (USA) flow cytometer

Software

CellQuest software

Cell population abundance

Parameters for data acquisition were kept constant for all samples. Sample flow rate was set at about 100 nuclei/s and at least 6000 nuclei were acquired for each sample.

Gating strategy

Densely gathered nuclei region in dot plot was gated and considered for final analysis to avoid unwanted counts. The average of coefficient of variation values (CV) for G1 peaks was used to evaluate the results. The results with CV<5% were considered as reliable.

☒ Tick this box to confirm that a figure exemplifying the gating strategy is provided in the Supplementary Information.